

広島大学学術情報リポジトリ  
Hiroshima University Institutional Repository

Title	Studies on the Structure of the Ryoke Metamorphic Rocks of the Kasagi District, Southwest Japan
Author(s)	HARA, Ikuo
Citation	Journal of science of the Hiroshima University. Series C, Geology and mineralogy , 4 (2) : 163 - 224
Issue Date	1962-11-15
DOI	
Self DOI	<a href="https://doi.org/10.15027/53009">10.15027/53009</a>
URL	<a href="https://ir.lib.hiroshima-u.ac.jp/00053009">https://ir.lib.hiroshima-u.ac.jp/00053009</a>
Right	
Relation	



# Studies on the Structure of the Ryoke Metamorphic Rocks of the Kasagi District, Southwest Japan

By

**Ikuo HARA**

---

*with 1 Table, 72 Text-figures, and 3 Plates*

---

**ABSTRACT:** Structural features on various scales of the Ryoke metamorphic rocks of the Kasagi district, Southwest Japan, were described and discussed, and the genetic history of geologic structure of the district was examined in connection with the plutonic and metamorphic history.

## CONTENTS

- I. Introduction
- II. Outline of Geology
- III. Mesoscopic Structures
  - A. Flexure folding of the bedding surface and the principal schistosity surface
  - B. Axial structures
  - C. Mesoscopic subordinate transversal surface
- IV. Macroscopic Structures
  - A. The Structure related to the Tamba deformation
  - B. The Structure related to the deformation during the Ryoke metamorphic phase
- V. Microscopic Structures
  - A. Microscopic conjugate transversal surfaces parallel to  $L_{2-3}$
  - B. Significance of the deformation related to the  $B_5$ -folds,  $L_5$  and the  $S_5$ -surfaces
  - C. Mica and quartz fabrics
- VI. Concluding Remarks
- References

## I. INTRODUCTION

The Kasagi district occupies the southern part of Kyoto Pref. and the northern part of Nara Pref., Southwest Japan. The district consists of the Ryoke metamorphic and granitic rocks, which belong to the Ryoke metamorphic zone. Within a few kilometers beyond the northern limit of the mapped area, the Ryoke metamorphic rocks are gradually changed to non-metamorphic rocks.

The basement geology of Southwest Japan is characterized by the zonal arrangement of older formations and their metamorphic equivalents, the latter divided into three metamorphic zones, *i.e.*, the Sangun, the Ryoke and the Sambagawa metamorphic zone. The Ryoke metamorphic zone is situated between the Sangun metamorphic zone to the north and the Sambagawa metamorphic zone to the south (Fig. 1). Between the Sangun and the Ryoke metamorphic zone lies a zone consisting mainly of non-metamorphic rocks of Palaeozoic groups, which suffered neither the Sangun nor the Ryoke metamorphism. This zone was named the intermediate non-metamorphic zone by G. KOJIMA (1953). In Kinki and Chubu province, however, the zone was named the Tamba zone by S. MATSUSHITA (1950) and N. YAMASHITA (1957).

In 1941, T. KOBAYASHI summarized the Palaeozoic and Mesozoic geology of Japan, and introduced a hypothesis that two great orogenic cycles can be distinguished: the older one is the Akiyoshi orogenic cycle (Late Palaeozoic~Early Mesozoic) and the younger one the Sakawa orogenic cycle (Middle~Late Mesozoic). After him, the Sangun metamorphic zone and the Hida zone represent the axial metamorphism of the Akiyoshi orogenic cycle, and the Ryoke and the Sambagawa metamorphic zone were formed during the Sakawa orogenic cycle. In 1952, M. GORAI discussed the origin of the Japanese Islands, and pointed out that the Ryoke and the Sambagawa metamorphic zone were also formed during the orogenesis of the Late Palaeozoic or the Early Mesozoic. GORAI's view has been supported by most of Japanese geologists, *e.g.*, KOJIMA (1953), YAMASHITA (1957) and K. ICHIKAWA (1958). Recently, data on the absolute age of granitic rocks in the Ryoke metamorphic zone and crystalline schist in the Sambagawa metamorphic zone have been reported by S. BANNO and J. MILLER (K-A method) (1961), and Y. KARAKIDA and D. GOTTFRIED (Lead-alpha method) (1961). All of those data gave the rocks in question the absolute ages corresponding to the Late Mesozoic. On the basis of this evidence, BANNO and MILLER claimed that the Ryoke and the Sambagawa metamorphic zone were formed during the orogenesis of the Late Mesozoic (*cf.* H. KUNO, 1961). In some places, the Upper Triassic system overlies unconformably the Sangun metamorphic rocks, that indicating without doubt the formation of Sangun metamorphic rocks during the orogenesis of the Late Paleozoic or the Early Mesozoic.

Therefore, it is very important to research the geology of the intermediate non-metamorphic zone which lies between the Ryoke and the Sangun metamorphic zone and to analyze the structural relation between the Ryoke metamorphic zone and the intermediate non-metamorphic zone.

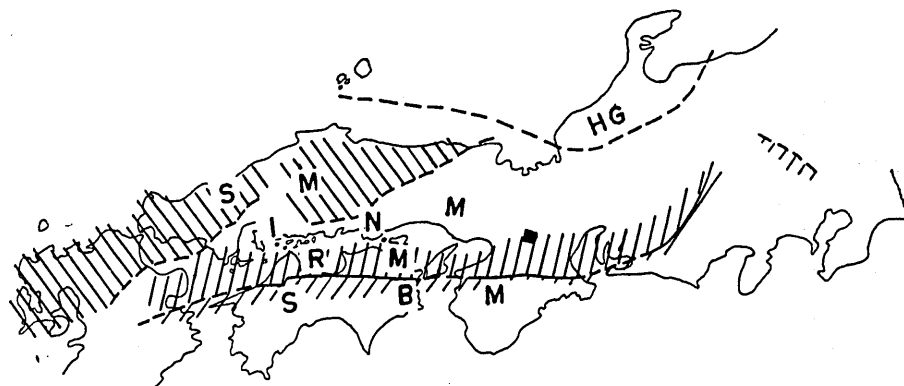


FIG. 1 Sketch map of zonal arrangement of older formations and their metamorphic equivalents in Southwestern Japan (after G. KOJIMA 1953).

HG: Hida gneiss complex, SM: Sangun metamorphic zone, INM: intermediate non-metamorphic zone, RM: Ryoke metamorphic zone, SBM: Sambagawa metamorphic zone. ■: Area investigated.

The geology of the Ryoke zone in Kinki province has been known poorly so far. Recently, W. NAKAZIMA (1960) published the geological outline map of the Ryoke zone in the Yamato Plateau, Central Kinki province. After his map (Fig. 2), the Ryoke metamorphic and granitic rocks have the east-west regional trend in the southern and northern margin of the Ryoke zone in the Yamato Plateau, subparallel to that of the Ryoke zone in Kinki and Chugoku province. While, in the central part of the Ryoke zone in the Yamato Plateau, principal schistosity and gneissosity surfaces of the Ryoke metamorphic and granitic rocks seem to form dome- and basin-like structures. The Kasagi district is situated on the transitional part between the northern and the central part with different regional trend of geologic structure as read from Fig. 2.

In this paper, the first purpose of the author is to study the structures on various scales of the Ryoke metamorphic rocks and further to determine the genetic history of the geologic structure in the Kasagi district.

The Ryoke zone is composed of metamorphic and granitic rocks, though in some places are developed igneous and sedimentary rocks which was formed after the Ryoke metamorphism had been ceased. KOJIMA (1953) said, "the Ryoke metamorphism is characterized by the prevalence of thermal and metasomatic effect closely related to intense plutonism. Metamorphic zones, commonly found in metamorphic regions of the normal regional metamorphic types such as chlorite, almandine, staurolite, and cyanite zones, are entirely absent in the Ryoke metamorphic zone. The metamorphic rocks are characterized by the minerals of thermal-metamorphic type such as andalusite, cordierite, sillimanite, etc." H. KOIDE (1949, 1958) studied the Ryoke metamorphic and plutonic rocks in the Dando district, Aichi Pref., especially from the petrochemical viewpoint. He discriminated between the older and the younger granodioritic intrusions and the associated metamorphism. He pointed out

that the older granodioritic intrusives were intruded successively after the older Ryoke metamorphism of regional extension had been completed. The main metamorphic area of the Dando district was classified by KOIDE into the following successive zones in relation to the older metamorphism, that is, the zone of schistose hornfels, the zone of transitional rocks, and the zone of banded gneiss. The younger metamorphic rocks seem to develop within narrow zone along the younger intrusives. Afterwards, similar relation with reference to the plutonism and metamorphism has been set forth in other districts of the Ryoke zone, *e.g.*, in the Yanai district by KOJIMA and OKAMURA (1951), and OKAMURA (1957), in the Kasagi district by T. ARITA (1949), in the Kiso Mountain Range by Y. OKI (1958) and M. KATADA et al., (1959), and in the Komagane district by Y. HAYAMA (1960), etc, that suggesting the prevalence of these types of plutonisms and metamorphisms throughout the Ryoke zone. The second purpose of the author is to define those two phases of plutonisms and associated metamorphism in terms of tectonic movement of the metamorphic field in the Kasagi district.

Microfabric patterns of quartz of the metamorphic rocks in the district have been classified by the author into four types. The significance of those types of the quartz fabric will also be discussed in this paper.

*Acknowledgements:* The author is extremely grateful to Professor G. KOJIMA for his constant guidance and encouragement kindly given to the author's field and laboratory works, and for reading the manuscript. The author also wishes to express his gratitude to Professors Y. KINOSAKI, S. IMAMURA, and Y. UMEGAKI for their continuous guidance and encouragement. Acknowledgements are due to Dr. K. HIDE for his suggestions and criticisms to the study. Thanks are also due to the members of the Petrologist Club of the Hiroshima University for their valuable discussions. Finally the author acknowledges with gratitude that a part of the expense for this research was defrayed by the Grant in Aid for Scientific Researches from the Ministry of Education, Japan.

## II. OUTLINE OF GEOLOGY

The Kasagi district consists of the Ryoke metamorphic and granitic rocks. As will be described in later pages, the sequence of tectonic movement in the district during the Ryoke phase has been divided into two main stages, *i.e.*, the older Ryoke deformation and the younger Ryoke deformation. With reference to those two stages of deformation the granitic rocks in the district are divided into three types as follows: 1) the Sakawa granodioritic rocks, which were intruded during the older Ryoke deformation, 2) the Yagyu granite which was intruded probably during and after the younger Ryoke deformation, and 3) the Koya granodioritic rocks which were intruded after the younger Ryoke deformation.

The Yagyu granite and the Koya granodioritic rocks effected thermal metamorphism in the rocks within narrower zones along them, though in the southern half

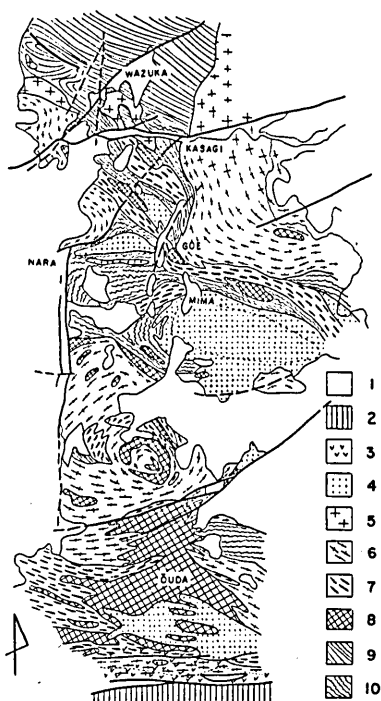


FIG. 2. Geological outline map of the Yamato Plateau of Central Kinki Province. (after W. NAKAZIMA (1960), but partially modified by the present author)

- 1 Post-Ryoke formations
- 2 Sambagawa metamorphic rocks
- 3 Mylonitic rocks
- 4 Fine-grained granitic rocks
- 5 Younger granitic rocks (massive)
- 6 Younger granitic rocks (gneissose)
- 7 Older granitic rocks
- 8 Metamorphic derivatives from basic rocks
- 9 Biotite-bearing slates
- 10 Schistose hornfelses and gneisses

younger granite" in the sense of KOIDE.

The original rocks of the metamorphic rocks consist mainly of pelite, semi-pelite, and banded chert, accompanied by subordinate sandstone, calcareous rock and basic volcanic rocks. In this district there can be found no palaeontological evidences for the age of those original rocks, but it seems probable that they may be of the Permo-Carboniferous age from their lithological natures which are remarkable similar to those of the Permo-Carboniferous rocks in the Tamba zone north of the district. Although the stratigraphy of original rocks has not yet been decided in detail, it may safely be said that pelite is predominant in the lower horizon (developing

of the district the thermal effect seems not so obvious as that in the northern half. The metamorphic rocks in the district, which has not suffered the thermal metamorphism by the Yagyu granite and the Koya granodioritic rocks, represent the products of the older Ryoke metamorphism. Broadly speaking, the older Ryoke metamorphic terrain of the district can be divided into three zones from the north to the south, *i.e.*, the zone of biotite-bearing slate (developing in subareas A, B and C in Fig. 4), the zone of schistose hornfels (developing mainly in subarea D) and the zone of gneiss (developing mainly in subareas E, F, G, H, I, J and K). Strictly speaking, however, in the zone of gneiss (subareas E, F, G, H and I) occurs schistose hornfels in pocket-like fashion, that being commonly away from the Sakawa granodioritic rocks. The zone of schistose hornfels is characterized by andalusite in the rocks of appropriate chemical composition, and the zone of gneiss by sillimanite. In the northern half of subarea E, both andalusite and sillimanite coexist. The Sakawa granodioritic rocks were intruded during the older Ryoke metamorphism. The Yagyu granite and the Koya granodioritic rocks correspond to "the

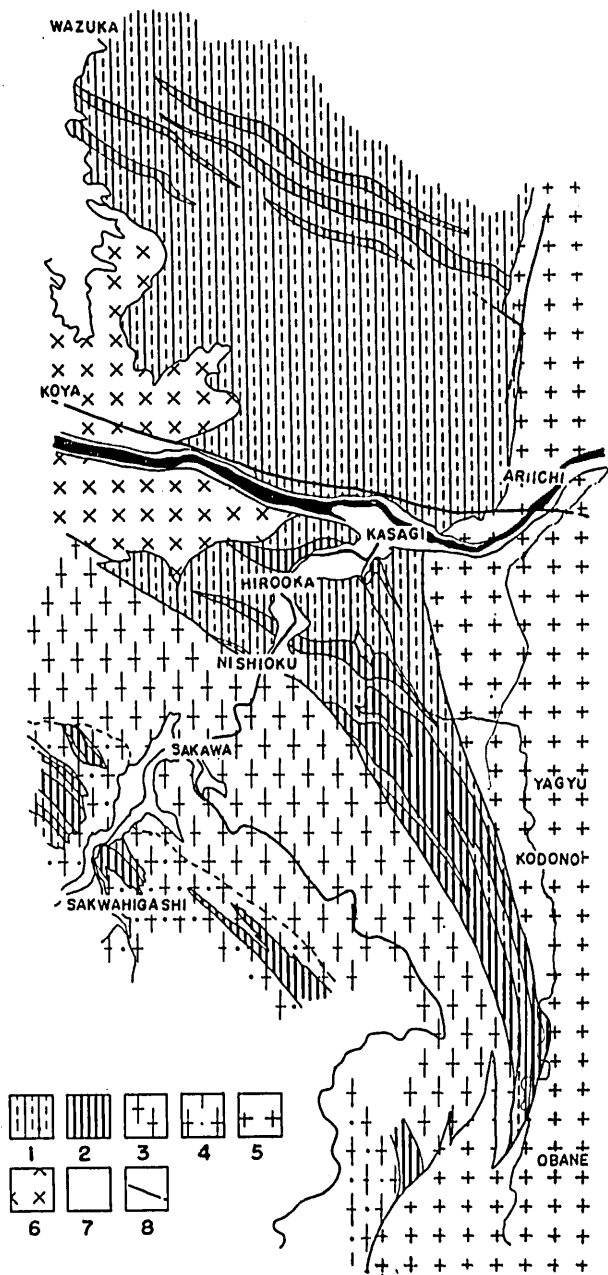


FIG. 3 Geological map of the Kasagi district.

- 1 Metamorphic derivatives from pelitic and semi-pelitic rocks
- 2 Metamorphic derivatives from banded chert
- 3 Sakawa granodiorite
- 4 Sakawa fine-grained granodioritic rocks
- 5 Yagyu granite
- 6 Koya granodioritic rocks
- 7 Cenozoic formations
- 8 Fault

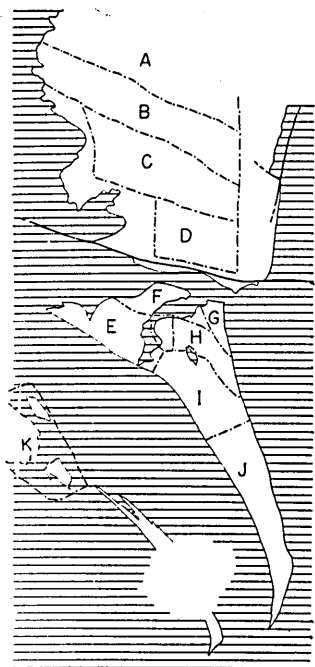


FIG. 4 Index map showing 11 subareas.

mainly in subareas C, D and G) and that in addition to pelite banded chert becomes predominant in the upper horizons (developing mainly in subareas A, B, E, F, H, I, J and K), especially in the apparently uppermost horizon (subarea K), which consists mostly of banded chert, as W. NAKAJIMA pointed out.

The Sakawa granodioritic rocks, which were intruded during the older Ryoke deformation, can be divided into two subtypes: 1) the Sakawa granodiorite—medium-grained biotite-granodiorite occurring as a large elongate mass in the southern half of the district (see geological map), and 2) the Sakawa fine-grained granodioritic rocks occurring as small masses, which vary petrographically from biotite-quartz-diorite to muscovite-biotite-granite. Boundaries between those

rock masses cannot be drawn as sharp lines, but they seem to grade petrographically as well as structurally each other.

Most of the Sakawa granodioritic rocks are characterized by marked linear and planar structures. The lineation is defined by remarkably elongated grains of quartz and feldspar (mainly plagioclase), and by parallel arrangement of biotite flakes. The planar structure develops rather weakly. The observed planar structure is a type of gneissosity defined by the preferred orientation of biotite flakes and by the elongation of grains of quartz and feldspar. Broadly speaking, the gneissosity surfaces trend parallel to the contact between the Sakawa granodioritic rocks and the metamorphic rocks, and also the trend of the lineation of the former having horizontal or gentle plunge is parallel or subparallel to that of the principal lineation (designated as  $L_{2-3}$ ; see the later pages) of the latter. Generally, the contact relation is conformable.

In some places, however, the Sakawa granodioritic rocks cut discordantly across the principal schistosity surfaces of the surrounding metamorphic rocks, and also, in some places of subarea K, the lineation of the Sakawa granodioritic rocks is remarkably oblique to the principal lineation ( $L_{2-3}$ ) of the surrounding metamorphic rocks. These evidences suggest that the Sakawa granodioritic rocks must be of the intrusive origin.

The gneissosity surfaces of the Sakawa granodioritic rocks cut generally across

aplitic and pegmatitic veins, and sometimes across "basic xenoliths" and xenoliths from the surrounding metamorphic rocks which generally show markedly elongate form parallel to the gneissosity surfaces. These facts suggest that the planar and linear structures of the Sakawa granodioritic rocks are not the structure of liquid flow, but that they are the "structure of the transition phase" in the sense of H. R. GAULT (1945) and M. R. BILLINGS (1942).

The Yagyu granite is widely exposed in the eastern area of the district. It is coarse-grained, hornblende-bearing biotite-granite. The structural features of the Yagyu granite change gradually from the south to the north. In the southern half of the mass of the Yagyu granite, there develops a gneissose feature defined by the parallel arrangement of mineral grains such as quartz, feldspar and biotite. This gneissose feature becomes gradually weak towards the north, and it becomes unrecognizable at Ariichi. Between Ariichi and Obane, the contact between the Yagyu granite and the metamorphic rocks is parallel or subparallel to the principal schistosity surfaces of the latter and to the gneissosity surfaces of the former. The metamorphic rocks within a narrow zone along the Yagyu granite between Ariichi and Obane show the slip cleavage which traverses the principal schistosity surface and is parallel or subparallel to the contact. The spacing of the slip cleavage tends to become narrow towards the contact. The slip cleavages is interpreted as formed by the forcible intrusion of the Yagyu granite. At about 500m to the north of Ariichi, where the Yagyu granite shows no gneissose feature, the contact relation changes suddenly to the discordant one.

The Koya granodioritic rocks, which were intruded subsequently to the younger Ryoke deformation, can be divided into two subtypes: 1) the Koya granodiorite—medium-grained biotite-granodiorite occurring as a large mass in the central area of the district (see geological map), and 2) the Koya fine-grained granodioritic rocks occurring as small masses in the metamorphic rocks and the Sakawa granodioritic rocks. They vary petrographically from biotite-quartz-diorite to muscovite-biotite-granite. The Koya granodioritic rocks were intruded, in general, discordantly into the surrounding rocks, and are free from planar and linear structures.

### III. MESOSCOPIC STRUCTURES

#### A. FLEXURE FOLDING OF THE BEDDING SURFACE, AND THE PRINCIPAL SCHISTOSITY SURFACE

##### 1. *General Statement*

Most of the metamorphic rocks (biotite-bearing slate to sillimanite-gneiss) within the district show a distinct schistosity surface, and are characterized by schistose feature. Especially, in those derived from pelitic and semi-pelitic rocks it is pronounced. Generally, the schistosity is defined by preferred orientation of mineral grains such as muscovite, biotite and amphibole, and by compositional banding as a result of metamorphic differentiation in some examples of gneiss, accordingly it in them corresponding to the foliation in the sense of A. HARKER (1932). In many of



FIG. 5 Relation between B<sub>1</sub>-fold (banded chert) and principal schistosity surface S<sub>1-2</sub>.



FIG. 6 B<sub>1</sub>-folds with décollement of banded chert (from subarea A)



FIG. 7 Structure of sandstone (stippled) and chert (lined) in incompetent pelite (from northern end of subarea A)

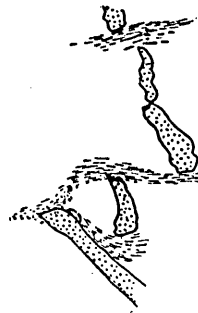


FIG. 8 Tectonic inclusions of sandstone (stippled) in incompetent pelite and principal schistosity surfaces S<sub>1-2</sub>. (from northern end of subarea A)

the rocks the schistosity surface is running parallel to the bedding surface, and siliceous gneisses derived from banded chert show a marked gneissic appearance composed of alternating bands of melanocratic and leucocratic compositions, reflecting original sedimentary variations. However, the schistosity surface is not always parallel to the bedding surface. As shown in Fig. 5 (cf. Plate 18-3), the former clearly cuts across the latter in many places. In such case, parallel arrangement of platy minerals along the bedding surface is not generally observed, or, if develops, weakly in gneiss. In many places, the schistosity surface cuts across the minor fold of the bedding surface, as shown in an example of Fig. 5, it suggesting that the latter had existed before the former was formed.

Now we will ask as follows: 1) What style was the deformation related to the folding of the bedding surface prior to the formation of the schistosity? 2) What relation between the former and the latter was there? and 3) Had the deformation related to the folding of bedding surface been accompanied with any recrystallization of mineral grains in the rocks concerned, accordingly also with the older Ryoke metamorphism, which was responsible for the formation of the older metamorphic rocks (biotite-bearing slate to sillimanite gneiss)?

On the basis of detailed examination of mesoscopic and microscopic structures of the rocks of the northern end of the district (corresponding to the zone of biotite-

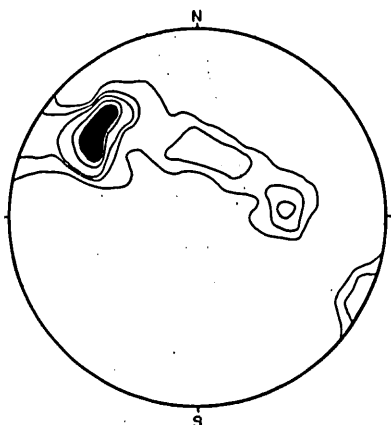


FIG. 9 Axes of the  $B_1$ -folds (of banded chert) in subareas A and B. Contours: 30-20-10-6-2%

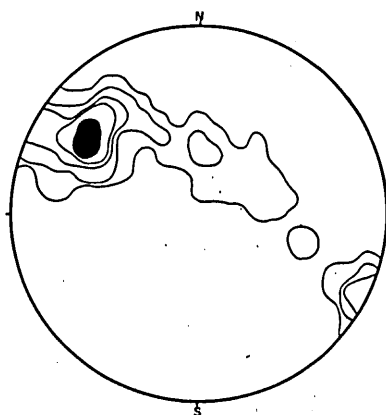


FIG. 10 Axes of the  $B_1$ -folds (of the competent beds in the pelitic and semi-pelitic rocks) in subareas A and B. Contours: 18-12-6-3-1.4%

bearing slate) and of the non-metamorphic rocks of the Tamba zone (in the vicinity of Uji, Kyoto Pref.) north of the district, it has been clarified that, prior to the older Ryoke metamorphism, the minor folding of the bedding surface had been produced with associated very slight recrystallization of mineral grains in the rocks concerned, and that the movement which produced the minor fold was that responsible for the formation of the schistosity mentioned above, but that the schistosity had been produced as S-surfaces ( $S'_1$ - and  $S''_1$ -surface) without associated available recrystallization of mineral grain along it in this deformation stage prior to the older Ryoke metamorphism, and that the parallel arrangement of mineral grains such as muscovite, biotite and amphibole defining the present schistosity owed to superposed shear movement on the S-surfaces during the Ryoke metamorphism. The evidence for those conclusions will be now discussed.

2.  $B_1$ -folds of metamorphic derivatives from banded chert in subareas A and B.

As a whole, the geologic structure of subareas A and B is for thick strata, which incline steeply towards NNE. In many places, however, the bedding surfaces of the rocks in those subareas are markedly folded on small-scale. Especially in banded chert, the degree of the small-scale folding is spectacular. In some places, tens of small-scale folds of banded chert (average wavelength 50cm) are laterally superposed in fashion of the close-packed. The small-scale folds of bedding surfaces of banded chert which were cut by the schistosity surface are designated as  $B_1$ -fold (Geometrical relation between the  $B_1$ -fold and schistosity surface will be described in later pages.)

The trends of the axes of  $B_1$ -folds are statistically illustrated in Fig. 9. Although it shows respectable variations, it can be pointed out that many of the fold-axes have the azimuth and plunge of ca.  $N48^\circ W$  and  $30^\circ$  respectively. In some exposures, the

$B_1$ -folds with various plunging axes coexist. In some of those exposures, they appear to surround large massive body of chert. And also in some places, the  $B_1$ -folds having the steeply plunging axes are refolded about an axis gently plunging towards NW. However, the diagram of Fig. 9 indicates that most of those fold-axes tend to spread on a great circle.

The attitude of the axial surfaces of folds is fairly regular and many of them seem to show trend approximately parallel to the great circle containing most of the fold-axes in the diagram of Fig. 9. However, the axial surfaces of folds are not always plane but often visibly curved.

In profile, the  $B_1$ -folds in question are commonly hardly curved, the turnover at the axis being sudded in acute angle, and rarely they show a moderate form. Pelitic material alternating with chert beds in the folds is commonly squeezed from their limbs into their axial zone, that suggesting flexural slipping involved in the bedding surfaces of competent chert. Some of the  $B_1$ -folds indicate a disharmonic style implying usually a certain amount of décollement (Fig. 6.) In those folds, generally, the one of limbs is straight and has markedly thinner thickness than other folded limb, as shown in Fig. 6 (cf. Plate 18-1). The surfaces of décollement generally develop in parallel along the former limb as shown in Fig. 6 and are controlled by the same tectonic axes as the folds. Most of  $B_1$ -folds show monoclinic symmetry, but some of them triclinic.

All folds described above are not associated by mylonite. Thus, the style of folds suggests that they had been formed in highly plastic condition of rocks concerned. The style of folds is not dissimilar to that of the Ord Ban quartzite described by D. B. McINTYER (1951). McINTYER said, "it is evident that quartzite can fold in this manner only if the quartz crystals are able to grow during the deformation . . . . ., recrystallization would give an effective plasticity to the mass as a whole." However, quite similar type of fold is frequently observed in the non-metamorphic banded chert in the Tamba zone north of the district. The  $B_1$ -folds in the district had been produced prior to the older Ryoke metamorphism, as will be discussed in later pages. Therefore, the deformation related to the formation of the fold in question seems to have taken place in the unconsolidated soft condition of the rocks concerned.

3. *Geometrical relation between the  $B_1$ -folds and schistosity surfaces in the banded chert in subareas A and B.*

The schistosity surfaces in question are running through the  $B_1$ -folds approximately parallel to their axial surfaces in many places. In this case, strictly speaking, they show fan-like arrangement with reference to the core of fold. However, in the  $B_1$ -folds implying décollement the schistosity surfaces are commonly parallel to the surfaces of décollement and to the straight thinner limb of folds. In the refolded folds as shown in Fig. 5, they are commonly approximately parallel to the axial surfaces of the fold in the later stage. Broadly speaking, the schistosity surfaces seem to show trend approximately parallel to the great circle containing most of the fold-axes in the diagram of Fig. 9.

From conformable geometrical relation between the  $B_1$ -folds and schistosity surfaces mentioned above, it may be concluded that the latter had been produced in close connection with the formation of the former and accordingly that the latter had been produced subsequently to the  $B_1$ -folding of bedding surfaces, though there are some problems which will be discussed in later pages.

4. *Folds and associated structures of the "competent" beds intercalated in the pelitic and semi-pelitic rocks in subareas A and B.*

The rocks, which behaved as competent beds with respect to the pelitic and semi-pelitic rocks surrounding them, are sandstone, chert and basic volcanic rocks. The principal rocks to be dealt with are the former one.

Broadly speaking, the sandstones appear to be intercalated as isolated tabular bodies on various scales rather than as extensive beds. At first sight, they appear to be scattered at random through pelitic and semi-pelitic rocks, though their long dimensions are generally oriented parallel to the general trend of strata indicated in the geological map. However, in many of profiles parallel to NNE, small-scale folds of the competent beds and folded orientation of their isolated bodies have been observed. The style of deformation of the competent beds (prior to the formation of the schistosity) will be discussed with reference to careful examination of those profiles.

The structures of competent beds in question are folding of bedding surface and structures such as mullion, boudin and tectonic inclusion. They indicate composite effects of those various styles of deformation. The development of those structures may be collectively interpreted as follows: in the earlier stage of deformation, competent beds are mullioned and boudinaged. In the more advanced stage, their continuities are destroyed into tectonic inclusions swimming in the incompetent matrix. Also the deforming process from mullioning and boudinage to the production of tectonic inclusions seems to have taken place contemporaneously during flexure folding of the beds, as suggested from example of Fig. 7. In some profiles, deforming process from flexure folding with boudins of competent beds, through folded orientation of their tectonic inclusions, to random orientation of these has been traced out. Most of observed folds show monoclinic symmetry, but some of them triclinic.

The style of the folds and associated structures described above suggests that they had been formed in highly plastic condition of rocks concerned. Similar structures have been observed also in the Tamba zone (in the vicinity of Uji, Kyoto Pref.) north of the district. They had been formed prior to the Ryoke metamorphism, as will be discussed in later pages. Therefore, the deformation related to the formation of the folds and associated structures of competent beds in question seems to have taken place in the unconsolidated soft condition of the rocks concerned.

Since the folds are complicated, it is often difficult to measure their axial trends and axial surfaces. The trends of all measured fold-axes are statistically illustrated in Fig. 10. Many of them show the azimuth and plunge of ca.  $N54^\circ W$  and  $28^\circ$  respectively. Those values are approximately equal to them for many of  $B_1$ -folds

of banded chert. Superposition of Fig. 9 on Fig. 10 shows that the great circle girdle containing most of the folds of competent beds coincides approximately with that for the  $B_1$ -folds of banded chert. The attitude of the axial surfaces of folds in question is fairly regular, and many of them show trend approximately parallel to the great circle in the diagram of Fig. 10. Thus, it is pointed out that the axial trends and axial surfaces of the folds in question show quite similar attitude to those of the  $B_1$ -folds of banded chert described in preceding pages.

Therefore, the  $B_1$ -folds of banded chert must be safely correlated with the above described folds and associated structures of the competent beds intercalated in the incompetent pelitic and semi-pelitic rocks. Thus, the small-scale folds of bedding surfaces in question (which are cut by the schistosity surface) are collectively designated as  $B_1$ -fold.

Apart from the structures described above, turbid laminations of the sandstone and semi-pelitic rocks in the pelitic rocks as shown in an example of Fig. 11 are observed in many places. They show no associated shear cleavage, and are cut irregularly by the schistosity surfaces. They must be



FIG. 11 An example of turbidity of the laminae of the pelitic (lined) and semi-pelitic rocks (from subarea A).  $S_{1-2}$ —  
— $S_{1-2}$ : showing the direction of the  $S_{1-2}$ -surfaces.

doubtlessly sedimentary structure, which indicates turbidity current of sediments concerned during sedimentation. In many places, however, the author could not always sharply distinguish between the  $B_1$ -folds and associated structures and those sedimentary structures. In the northern end of the district has been observed development of pelitic fragments incorporated as separate pieces in sandstone beds, which can be doubtlessly attributed to turbidity current of sediments concerned during sedimentation.

5. Geometrical relation between the  $B_1$ -folds of intercalated competent beds and schistosity surfaces in the pelitic and semi-pelitic rocks in subareas A and B.

Generally, the schistosity surfaces in question tend to run in approximately parallel to the axial surfaces of the  $B_1$ -folds of competent beds. They only weakly develop in the competent rocks. Especially, the development of the schistosity is insignificant in these rocks of subarea A. While, the schistosity surfaces well develop in the incompetent pelitic and semi-pelitic rocks. About the development of them in these rocks of subarea A, however, following evidences have been recognized: where the form of the  $B_1$ -folds of competent beds well remains, the development of the schistosity is relatively weak to that in places, where the competent beds are disrupted to such extent that it becomes difficult to trace out the form of the fold. In some of the former cases, the schistosity surfaces are recognized only along the zones of separation of the boudins and run in approximate parallel to those zones in such fashion as shown in example of Fig. 8. Those schistosity surfaces seem to be controlled by the

same tectonic axes as the  $B_1$ -folds. Rocks of remaining parts are rather massive, and flaky minerals such as muscovite and biotite seem to be oriented on sedimentary liminae rather than are parallel to the axial surface of the fold concerned.

Mesoscopic structures, which have been described in preceding pages, were traced out in quite similar fashion from subarea A to Uji, Kyoto Pref., in the Tamba zone north of the district. Only the schistosity surfaces are gradually changed to S-surfaces (followingly designated as  $S'_1$  and  $S''_1$ ) in the Tamba non-metamorphic zone, which show scarcely parallel orientation of mineral grain along them. The rocks in the Tamba zone show a planar structure defined by parallel arrangement of very fine matters, one of which is very fine grained recrystallized white mica, that representing slight recrystallization of the rocks concerned. The planar structure is not always parallel to the bedding surface. This is designated as  $S'_1$ . In the structure of style as shown in Fig. 8, the  $S'_1$ -surfaces are parallel to displacement zones. The rocks in the Tamba zone have another distinct planar structure running parallel to or subparallel to the  $S'_1$ -surfaces. This planar structure is swarm of shear cleavages with length of order of millimeter (here termed  $S''_1$ ). Slip movement along the  $S''_1$ -surfaces seem to have been commonly negligible. Therefore, swimming of tectonic inclusions of competent rocks in the incompetent matrix seems to be attributable to highly plastic flow of the matrix with respect to  $S'_1$ , but not to slip movement with respect to the  $S''_1$ -shear cleavages. However, the  $S''_1$ -shear cleavages seem to be controlled by the same tectonic axes as the folds of competent beds. Thus, it seems probable that the movement, which produced the  $B_1$ -folds and associated structures for the competent beds, was that responsible for the formation of the  $S''_1$ -shear cleavage. The formation of  $S''_1$ -shear cleavage may be ascribed to decrease of plasticity of the rocks concerned in the later stage of deformation, probably owing to escape of water from the rocks concerned with progress of deformation (WUNDERLICH, 1959). Fig. 12 shows the  $c$ -axes fabric of quartz in the psammitic rock with the  $S'_1$ -

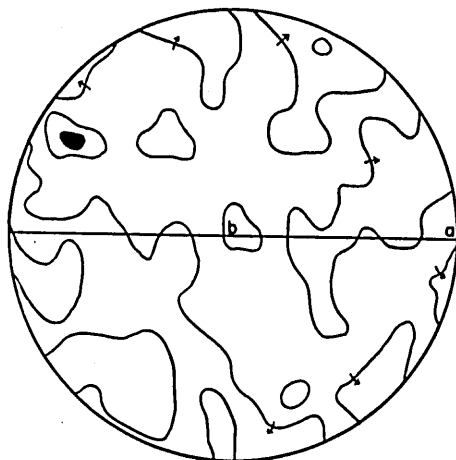


FIG. 12 400  $c$ -axes of quartz in psammitic rock collected from Uji; contours 3-2-1%

and  $S'_1$ -surfaces ( $S'_1/S_1$ ) collected from Uji in the Tamba zone. Random orientation of quartz axes is demonstrated. It is safely pointed out that the deformation related to the formation of the  $S'_1$  and  $S''_1$ -surfaces had not induced lattice translation of quartz, and in the plastic flow of the rock concerned with respect to the  $S'_1$ -surfaces the quartz grains floated in matrix. Those conclusions may be valid also for the structures in question in subarea A.

#### 6. Concluding remarks

On the basis of examination of deformation style, it may be concluded that the deformation, which produced the minor flexure folds ( $B_1$ -fold) and associated structures of the banded chert and the competent beds intercalated in the pelitic and semi-pelitic rocks, had taken place in unconsolidated soft condition of sediments concerned. Those structures are markedly similar to structures attributed to movement during sedimentation, such as intraformational folds and slumps. They may be sedimentary structure, which indicates turbidity current of sediments concerned during sedimentation, as well as the development of pelitic fragments incorporated as separate pieces in sandstone beds and other structures such as the example of Fig. 11. However, many of the structures in question seem not to be sedimentary structure, judging from conformable geometrical relation between them and schistosity surfaces and the evidences discussed in other chapter. Above described relationship between the  $S'_1$ - and  $S''_1$ -surfaces in the rocks of the Tamba zone seems to confirm this conclusion. In subareas A and B, as a whole, the  $b$ -kinematic axis in the deformation related to the formation of the structures in question have azimuth and plunge of ca.  $N48^\circ-54^\circ W$  and  $30-28^\circ$  respectively, as suggested from Figs. 9 and 10.

Analogous minor folds of bedding surface and associated structures and also analogous geometrical relation between the folds and schistosity surfaces have been recognized in many places of other subareas, especially in derivatives from the banded chert. They generally show complicated style, because of superposition of deformations accompanied with intense thermal and metasomatic effects. It is obvious that, prior to the formation of the schistosity surfaces, the rocks in those subareas had been deformed in the same manner as those in subareas A and B.

The evidences for the conclusions mentioned in the section of General statement will be further discussed in other sections and chapters.

In this paper, the bedding surface is designated as  $S_1$ . The schistosity surface in question is designated as  $S_{1-2}$  (or principal schistosity), on the basis of geometrical relation of it to  $S_1$  described in preceding pages. The axis of the  $B_1$ -fold is designated as  $L_1$ , and the line of intersection of  $S_1$  and  $S_{1-2}$  as  $L_{1-2}$ . Generally  $L_1$  is parallel to  $L_{1-2}$ .

### B. AXIAL STRUCTURE

#### 1. $L_1$ and the principal lineation $L_{2-3}$ .

Most of the metamorphic rocks within the district show a distinct lineation defined by parallel arrangement of mineral grains such as micas and amphibole on the

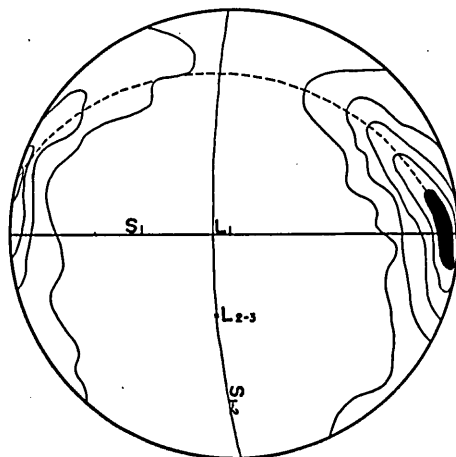


FIG. 13  $200 [001]$  of micas of slightly metamorphosed banded chert (from Kamatsuka)  
Contours: 15-13-9-7-1%

schistosity surface  $S_{1-2}$ . In subarea A, the northern part of the district, however, development of the lincation is insignificant, though it becomes progressively distinct towards the south. The lincation is designated as the principal lincation or  $L_{2-3}$ , since it coincides with the line of intersection of  $S_{1-2}$  and subordinate transversal-schistosity surfaces  $S_3$  and  $S_4$ , as will be discussed in later pages.

The  $L_{2-3}$ -lincation is first direct expression of the  $b$ -kinematic axis with respect to shear movement on  $S_{1-2}$ . Transposition of  $S_1$  by slip on  $S_{1-2}$  is observed in many places. However,  $L_{1-2}$  (the line of intersection of  $S_1$  and  $S_{1-2}$ ) is the fabric  $b$  in the symmetrolological system. Broadly speaking,  $L_{1-2}$  is oblique to  $L_{2-3}$  with an average angle of ca.  $25^\circ$  on  $S_{1-2}$ . Generally  $L_{1-2}$  is parallel to  $L_1$ . In the preceding pages, it has been pointed out that the movement which produced the  $B_1$ -folds (flexure fold) was probably that responsible for the formation of  $S_{1-2}$ , from the examination of geometrical relation between both structures in subareas A and B. Thus, problem about the relation between the flexure folding of bedding surfaces (the formation of the  $B_1$ -folds) and formation of  $S_{1-2}$ -schistosity seems to be remarkably intricate. The problem will be discussed in the chapter IV.

Where  $L_{2-3}$  runs obliquely to  $L_{1-2}$ , generally, arrangement of mineral grains such as muscovite and biotite parallel to  $L_{1-2}$  on  $S_{1-2}$  has been not megascopically observed. Fig. 13 shows the  $[001]$ -fabric of muscovite and biotite in the  $B_1$ -fold of banded chert in Kamatsuka of subarea A. In this specimen,  $L_1$  is parallel to  $L_{1-2}$ , and  $L_1$  is oblique to  $L_{2-3}$  with angles of ca.  $30^\circ$  on  $S_{1-2}$ .  $[001]$ -Axes of muscovite and biotite have been measured in thin section perpendicular to  $L_1$  and  $L_{1-2}$ . Fig. 13 is characterized by an incomplete girdle perpendicular to  $L_{2-3}$  and one maximum which corresponds to  $S_{1-2}$ . Marked flexure folding of  $S_1$  can not be traced out by the mica-fabric. Analogous pattern of mica-fabric with reference to  $L_{1-2}$  and  $L_{2-3}$  is equally obvious in examples from other places. In the example of Fig. 13, the  $S_{1-2}$ -surfaces

retain fan-like arrangement with reference to the core of fold, and the  $L_{2-3}$ -lineation is faint. In subarea A, as a whole, the  $S_{1-2}$ -surfaces are rotated about  $L_1$ , as will be described in the chapter IV. On the basis of those considerations, it seems to be safely concluded that muscovite and biotite in the metamorphic rocks within the district had originated first in the stage of deformation related to the formation of the principal lineation  $L_{2-3}$ , and therefore that the movement which produced the  $B_1$ -folds and associated structures described in preceding pages had taken place in non-metamorphic condition, that is, prior to the Ryoke metamorphism. The movement (prior to the Ryoke metamorphism) is named Tamba deformation in such points of view as will be discussed in the later pages (HARA, 1959, 1960).

2. *Minor folds of the  $S_{1-2}$ -surfaces having their axis parallel to  $L_{2-3}$ .*

In subareas A and B, as a whole, the  $S_{1-2}$ -surfaces are plane or weakly wavy. However, they often show visibly wavy form around tectonic inclusions of competent rocks in the pelitic and semi-pelitic rocks. Analogous attitude of the  $S_{1-2}$ -surfaces has been more or less observed all over the district.

In subareas C and D, the  $S_{1-2}$ -surfaces show commonly gentle waves, in some places accompanied with minor flexure folding in obtuse angle. Those folds show trend parallel to  $L_{2-3}$ .

While, in subareas E to K the  $S_{1-2}$ -surfaces are folded on every scale rather than are plane. The folds in those subareas are classified into three groups with reference to the attitude of their axes to  $L_{2-3}$  and named as follows in the order of younging: 1)  $B_3$ -folds trending in parallel to  $L_{2-3}$ , 2)  $B_5$ -folds trending slightly obliquely to  $L_{2-3}$ , and 3)  $B_6$ -folds having their axes plunging at high angles (accordingly, perpendicular or subperpendicular to  $L_{2-3}$ ). The most frequently observed folds are the  $B_3$ -folds. Some of the important mesoscopic features of the  $B_3$ -folds will be described.

The  $B_3$ -folds are concentric rather than similar (in the sense of De SITTER, 1956). They show various styles ranging from gentle or moderate form with orthorhombic or monoclinic symmetry to isoclinal-disharmonic, ptigmatic form with monoclinic symmetry. Most of the folds show monoclinic symmetry, but some of them show triclinic symmetry, owing to overprinting of the  $B_5$ -folds or  $B_6$ -folds. The attitude of the axial surfaces of  $B_3$ -folds is variable. However, its variation seems to be closely connected with that in the style of the  $B_3$ -folds. The axial surfaces of the  $B_3$ -folds showing gentle or moderate form tend to dip steeply with their subparallel arrangement within small area. On the other hand, the attitude of the axial surfaces of  $B_3$ -folds showing acute form is rather variable, as well as those of disharmonic style. All types of the  $B_3$ -folds occur all over subareas E to K. However, the  $B_3$ -folds showing moderate form are found most frequently in subareas F, H, I, and J. The  $B_3$ -folds showing isoclinal-disharmonic style are found most frequently in subarea K, and in the peripheral zones of the Sakawa granodioritic rocks.

### 3. Axial structures trending slightly obliquely to $L_{2-3}$ .

In some places of subareas C and D, other lineation oblique to  $L_{2-3}$  at angles varying from  $10^\circ$  to  $40^\circ$  has been observed on  $S_{1-2}$  (Fig. 18). This is represented by faint parallel striations or grooves. This type of lineation has not been observed in subarea A. It cannot be directly determined whether the striations and grooves on  $S_{1-2}$  in question correspond to the  $b$ -kinematic axis or not. They are designated as  $L_5$ . Azimuths of  $L_5$ -lineations deviate commonly towards the north with small angles to  $L_{2-3}$ .

In subareas E to K, the folds of the  $S_{1-2}$ -surfaces trending slightly obliquely to  $L_{2-3}$ , namely the  $B_5$ -folds, occur sporadically on small-scale. Most of them are found in the peripheral zones of the Sakawa granodioritic rocks.

The  $B_5$ -folds are concentric rather than similar in type (in the sense of De SITTER, 1956). The  $B_5$ -folds show various styles ranging from moderate form to isoclinal-disharmonic, ptygmatic form. Most of them show monoclinic symmetry, but others orthorhombic or triclinic symmetry. The style of  $B_5$ -folds is similar to that of the  $B_3$ -folds.

Some of the  $B_5$ -folds are accompanied by the lineation parallel to their axis in the axial zones, it defined by the parallel arrangement of mineral grains such as muscovite and biotite or by parallel striations. From tectonic sequence printed on  $S_{1-2}$ , the  $B_5$ -folds and the lineation seem to be correlated with  $L_5$  in subareas C and D.  $L_5$  may be regarded as the  $b$ -kinematic axis with respect to superposed shear movement on the  $S_{1-2}$ -surfaces, which in subareas C and D had taken place during the deformation stage, when the  $B_5$ -folds were formed in subareas E to K. On the basis of these considerations, in this paper, all those lineations described above are collectively designated as  $L_5$ .

Broadly speaking, however, the development of  $L_5$  and the  $B_5$ -folds is insignificant. This fact suggests that the shear movement on the  $S_{1-2}$ -surfaces related to the formation of  $L_5$  and the  $B_5$ -folds had taken place sporadically within the district, or that the shear movement had taken place with the  $b$ -kinematic axis parallel to  $L_{2-3}$  in other many places within the district where  $L_5$  and  $B_5$ -fold have not been recognized. The latter inference seems to be more probable, judging from the evidence described in the later pages.

### 4. Axial structures plunging at high angles.

Axial structures in question are the  $B_6$ -folds and the steeply plunging lineation defined by the parallel arrangement of mineral grains such as muscovite, biotite and amphibole on  $S_{1-2}$ . The lineation is designated as  $L_6$ . The  $B_6$ -folds and  $L_6$  have been mainly observed on the  $S_{1-2}$ -surface inclining at angles of between  $40^\circ$  and  $90^\circ$  in subareas F to K. Generally their trends coincide approximately with the direction of dip of  $S_{1-2}$ . Accordingly, they tend to run perpendicular to  $L_{2-3}$ , though not strictly perpendicular to  $L_{2-3}$ .

The style of most of the  $B_6$ -folds is that of the "drag fold" on small-scale. In

many places,  $L_6$  develops in close association with the  $B_6$ -folds. In places, however, where no  $B_6$ -folds can be seen,  $L_6$  persists. In subareas F, G and H, and the norther half of subarea J, the  $B_6$ -folds occur generally in the derivatives from the pelitic and semi-pelitic rocks. In the derivatives from banded chert of those subareas,  $L_6$  has been recognized.

The development of the  $B_6$ -folds as drag fold suggests that shear movement on the  $S_{1-2}$ -surfaces with respect to the horizontal or gently plunging  $a$ -kinematic axis had taken place in rocks of subareas F to K.  $L_6$  corresponds also to the  $b$ -kinematic axis with respect to the shear movement in question. In subareas G, H and I, the sense of shear movement on the  $S_{1-2}$ -surfaces determined from careful examination of the form of  $B_6$ -folds, as a whole, is what the eastern side moves towards the north relatively to the western side.

### C. MESOSCOPIC SUBORDINATE TRANSVERSAL SURFACE

In some places of the closely peripheral zones of the Sakawa granodioritic rocks, planar structural surfaces which traverse the  $S_{1-2}$ -surfaces and are generally displayed as one set of transversal surface with spacing of 3cm+ have been observed. Especially, they are found most frequently in subarea K. The development of the transversal surfaces in question, however, as a whole, is insignificant.

The transversal surfaces in question are commonly defined by parallel orientation of platy minerals such as micas and lensoid forms of quartz grains. Accordingly, they correspond to the schistosity in the sense of HARKER. Generally, the transversal surfaces are recognized as a zone with width of between 1mm and 2cm, in which the  $S_{1-2}$ -surfaces disappear completely, as shown in Plate 20-2. In some of the transversal surfaces rotation of platy minerals from  $S_{1-2}$  to them is incomplete. Those

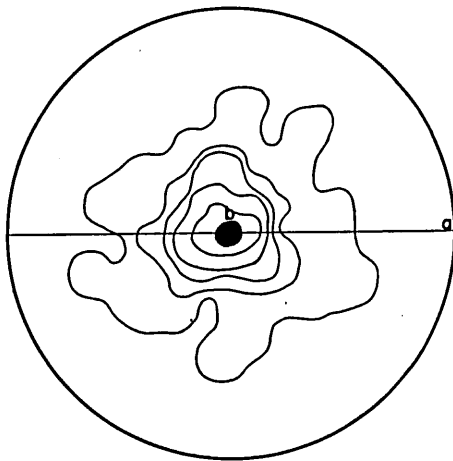


FIG. 14 100  $c$ -axes of sillimanite in the zone of  $S_5$ -surfaces (from Sakawahigashi); contours 30-25-15-7-3-1%

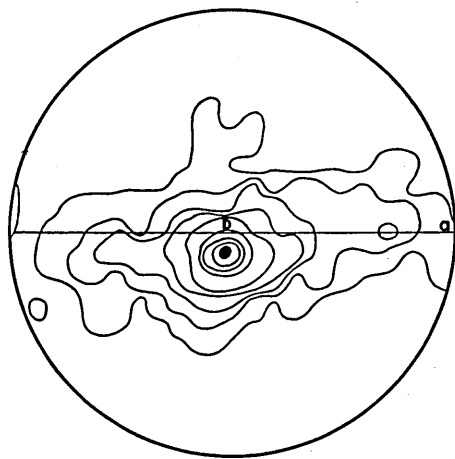


FIG. 15 100  $c$ -axes of sillimanite in the zone of  $S_7$ -surfaces (from Sakawahigashi); contours 15-13-11-9-7-5-3-2-1%

transversal surfaces are collectively designated as  $S_5$ .

The presence of  $S_5$ -schistosity surfaces developing in zones with wide width suggests considerable shear movement on them. On the  $S_5$ -surfaces of those zones, a distinct lineation is generally recognized. The lineation is defined by parallel arrangement of mineral grains such as muscovite and biotite commonly, and sillimanite sometimes. In some specimens, another microscopic planar structural surfaces, which traverse  $S_5$  and are represented by parallel sets of slip zones, have been recognized. The line of intersection of the  $S_5$ -surfaces and the microscopic transversal surfaces coincides with the lineation defined by parallel arrangement of mineral grains such as micas and sillimanite (Figs. 14 & 15). Those lineations are parallel to the line of intersection of  $S_{1-2}$  and  $S_5$ . Those lineations are collectively designated as  $L'_5$ . Where the  $S_5$ -surfaces and  $B_5$ -folds coexist,  $L'_5$  seems to be parallel to the axes of  $B_5$ -folds.

The movement which produced the  $B_5$ -folds may have been that responsible for the formation of  $S_5$ , and the  $S_5$ -surfaces may have been subsequently produced in the later stage of the deformation related to the  $B_5$ -folds.

Figs. 14 and 15 show the  $c$ -axis fabric of sillimanite in the zone of  $S_5$ -surfaces. Both diagrams are characterized by a single marked maximum, representing that the  $c$ -axes of sillimanite are preferably oriented in parallel to the fabric axis  $b$  ( $L'_5$ ).

#### IV. MACROSCOPIC STRUCTURES

##### A. THE STRUCTURE RELATED TO THE TAMBA DEFORMATION

In subareas A and B, as a whole, the  $S_{1-2}$ -surfaces tend to dip at high angles towards NNE. In subarea C, the  $S_{1-2}$ -surfaces change gradually their inclination towards SSW, but generally, they seem to have steep inclination. In subareas D they tend to dip with various angles towards SSW. The variation in the inclination of  $S_{1-2}$ -surfaces within subarea C seems, however, not to be attributed to the presence of anticlinal form with respect to  $S_{1-2}$ . Passing from the north to the south, they seem to change their inclination gradually from high angles towards NNE, through vertical position, to high angles towards SSW.

The trend of the  $S_{1-2}$ -surfaces in the pelitic and semi-pelitic rocks within subareas A to D is shown in Fig. 16. The  $\pi$ -diagram for  $S_{1-2}$  has been constructed by projecting poles of  $S_{1-2}$  on the lower hemisphere of equal-area-projection. The diagram is characterized by two prominent maxima and a single great circle girdle containing one of those maxima. It can safely be said that, as a whole, the structure of the  $S_{1-2}$ -surfaces within subareas A to D shows triclinic symmetry. The Maximum ( $M_1$  in Fig. 16), which is situated away from the great circle girdle, indicates the constancy in the trend of  $S_{1-2}$  in the pelitic and semi-pelitic rocks in subareas A and B.

Fig. 19-a is the  $\beta$ -diagram for  $S_{1-2}$  in the pelitic and semi-pelitic rocks in subarea A. The diagram has been constructed after the method of B. SANDER (1948). The diagram is characterized by a single marked maximum, though the  $\beta$ -axes show

considerable dispersion on a great circle. Accordingly, it may be pointed out that, on macroscopic scale, the structure of the  $S_{1-2}$ -surfaces in subarea A has a monoclinic symmetry with a single symmetry plane normal to the  $\beta$ -maximum, on the basis of consideration about the attitude of  $S_{1-2}$  described in preceding pages. The azimuth and plunge of the  $\beta$ -maximum are  $N48^\circ W$  and  $30^\circ$ , respectively.  $L_{2-3}$ -lineations in subarea A, plotted in Fig. 19-b, show a distinct maximum. The azimuth and plunge of the maximum are  $N55^\circ W$  and  $5^\circ$ , respectively. Therefore, the trend of  $L_{2-3}$  does not coincide with that of the  $\beta$ -maximum. While, the general trend of the axes of the  $B_1$ -folds in subareas A and B described in preceding pages coincides approximately with that of the  $\beta$ -maximum in question. This fact is quite harmonic with the conclusion deduced from the analysis of the mesoscopic structures in the chapter III, that the movement which produced the  $B_1$ -folds might have been that responsible for the formation of the  $S_{1-2}$ -surfaces.

Figs. 21-a and 22-a are the  $\beta$ -diagram for  $S_{1-2}$  in the pelitic and semi-pelitic rocks in subareas C and D, respectively. Those diagrams are characterized by a single marked maximum in common. Especially, it is pronounced in the  $\beta$ -diagram for subarea D. The trend of the  $\beta$ -maximum is constant with the azimuth and plunge of  $N73^\circ W$  and  $0^\circ$  in subarea C, and those of  $N75^\circ W$  and  $0^\circ$  in subarea D.  $L_{2-3}$ -lineation measured in those subareas have been plotted in Figs. 21-b and 22-b, both showing a single distinct maximum having quite similar trend. The azimuth and plunge of the maximum in both diagrams are  $N74^\circ W$  and  $0^\circ$  respectively. Therefore, in those subareas, the trend of  $L_{2-3}$  coincides with that of the  $\beta$ -maximum. Accordingly, it is safely concluded that, on macroscopic scale, the structure of the  $S_{1-2}$ -surfaces in subareas C and D shows monoclinic symmetry with a single symmetry plane normal to the  $\beta$ -maximum, on the basis of consideration about the attitude of  $S_{1-2}$ -surfaces within those subareas described in preceding pages, and that it is attributed to the deformation related to the formation of the lineation  $L_{2-3}$ .

Fig. 20-a is the  $\beta$ -diagram for  $S_{1-2}$  in the pelitic and semi-pelitic rocks in subarea B. The diagram is characterized by two prominent maxima. The azimuth and plunge of the one of them ( $M_1$ ) are  $N50^\circ W$  and  $32^\circ$  respectively, and the direction coincides well with that of  $L_1$  in subareas A and B shown in Fig. 10. The azimuth and plunge of the other  $\beta$ -maximum ( $M_2$ ) are  $N70^\circ E$  and  $3^\circ$  respectively. Preferred orientation of  $L_{2-3}$  in subarea B is illustrated in Fig. 20-b. A distinct maximum in the diagram shows the azimuth and plunge of  $N66^\circ W$  and  $3^\circ$  respectively. The trend of the  $\beta$ -maximum ( $M_2$ ) coincides approximately with that of the  $\beta$ -maximum and that of  $L_{2-3}$  in subareas C and D, but does not coincide with the trend of  $L_{2-3}$  in the same subarea B. We can say, however, that the  $\beta$ -maximum ( $M_2$ ) and  $L_{2-3}$  in subarea B have fairly identical trend.

On the basis of evidence described above, the structure of the  $S_{1-2}$ -surfaces in subareas A to D will be interpreted as follows. The formation of the structure of the  $S_{1-2}$ -surfaces in subarea A, which is characterized by their steep inclination towards NNE, may be ascribed to the deformation, which produced the  $B_1$ -folds and

associated structures of the banded chert and the competent beds intercalated in the pelitic and semi-pelitic rocks described in the chapter III. Accordingly, it may be safely concluded that main rock-structures and geologic structure in subarea A were produced during the Tamba deformation. The development of  $L_{2-3}$  on the  $S_{1-2}$ -surfaces suggests, however, the superposition of deformation produced the preferred orientation of mineral grains such as muscovite and biotite on  $S_{1-2}$  as shown in Fig. 13, though it seems to have been not so significant with respect to the destruction of mesoscopic and macroscopic structures in subarea A, which had been produced during the Tamba deformation.

As mentioned in the chapter III, mesoscopic structures related to the Tamba deformation have been recognized in many places within the district. This fact suggests that the Tamba deformation took place widely throughout the district. Structural features on various scales observed in subarea A can be traced in quite similar fashion from the subarea A to Uji, Kyoto Pref., in the Tamba zone north of the district, although the  $S_{1-2}$ -surfaces in the Tamba zone show features of  $S'_1$ - and  $S''_1$ -surfaces described above, practically scarcely accompanied by the parallel arrangement of mineral grains on them. As analysed in the chapter III, the rocks within the district too seem not to have experienced noticeable recrystallization of constituent mineral grains during the Tamba deformation. Therefore, it is concluded that the  $S_{1-2}$ -surfaces within the district, which at present are characterized by marked parallel arrangement of mineral grains such as muscovite and biotite, were produced as  $S'_1$ - and  $S''_1$ -surfaces during the Tamba deformation, just as shown in the Tamba zone, on the basis of considerations about geometrical relations between  $S_{1-2}$  and  $B_1$ -folds described in preceding pages. The  $b$ -kinematic axis with respect to the formation of the incipient  $S_{1-2}$ -surfaces (=  $S'_1$ - and  $S''_1$ -surface) during the Tamba deformation must coincide with  $L_1$  and  $L_{1-2}$ .  $L_{2-3}$ -lineation on  $S_{1-2}$ -surfaces must be correlated with the  $b$ -kinematic axis with respect to the superposed shear movement on  $S_{1-2}$  during the older Ryoike metamorphism. Thus, it may be concluded that similar rock- and geologic structures, to what are observed in the vicinity of Uji in the Tamba zone at present, developed all over the district prior to the Ryoike metamorphism.

The effect of superposition of the deformation related to the formation of  $L_{2-3}$  becomes progressively distinct, passing from subarea A to subarea D, and the structure of subarea C and D, especially that of the latter, is homogeneous with respect to  $\beta$ -axis parallel to  $L_{2-3}$ . This fact indicates that the structure of the  $S_{1-2}$ -surfaces in these subareas had been completely reconstructed by the deformation related to the formation of  $L_{2-3}$ -lineation during the Ryoike metamorphism, as in the case for subareas E to K that will be described in later pages.

W. NAKAJIMA (1960) assumed a large anticlinal fold with reference to the attitude of the  $S_{1-2}$ -surfaces in subarea C, and named the Wazuke anticline. He described a large anticlinal fold shown by thick beds of banded chert near Mt. Ōyake west-north-west of subarea C (parallel to the direction of strike of  $S_{1-2}$ ) in his geological



FIG. 16  $\pi$ -diagram for  $S_{1-2}$  of biotite-bearing slate and schistose hornfels in subareas A, B, C and D. Contours: 12-10-8-6-4-2-0.6%

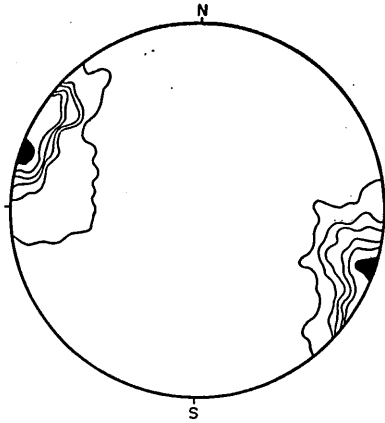


FIG. 17  $L_{2-3}$  of biotite-bearing slate and schistose hornfels in subareas A, B, C and D. Contours: 35-27-17-10-3-0.77%

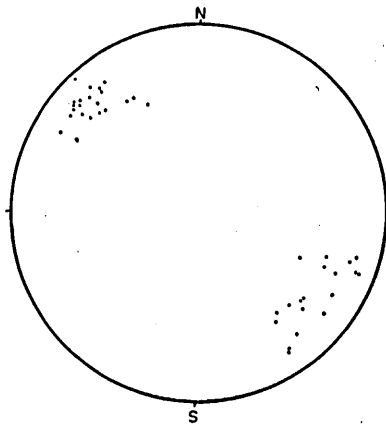


FIG. 18  $L_5$  of schistose hornfels in subareas C and D

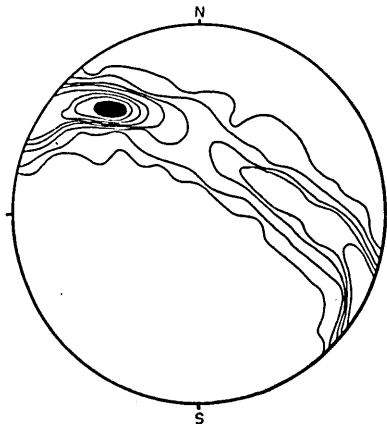


FIG. 19 a)  $\beta$ -diagram for  $S_{1-2}$  of biotite-bearing slate in subarea A. Contours: 16-12-10-8-6-4-2-1/2.5%

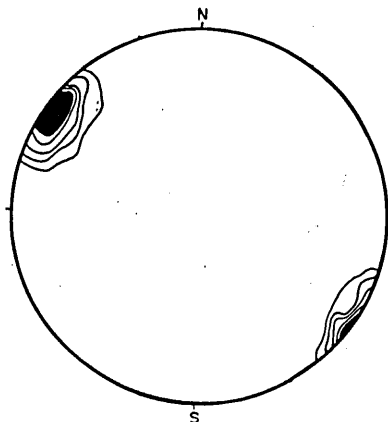


FIG. 19 b)  $L_{2-3}$  of biotite-bearing slate in subarea A. Contours: 40-30-20-10-3.3%

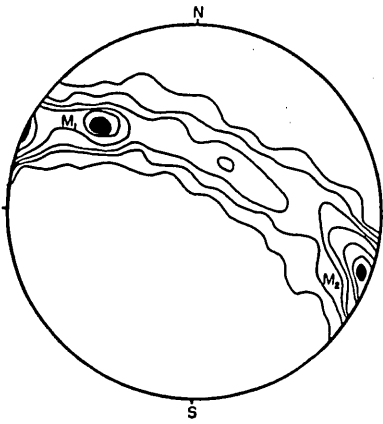


FIG. 20 a)  $\beta$ -diagram for  $S_{1-2}$  of biotite-bearing slate in subarea B Contours: 10-8-6-4-2-1/2.5%

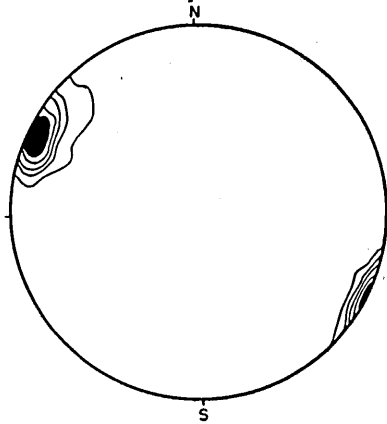


FIG. 20 b)  $L_{2-3}$  of biotite-bearing slate in subarea B Contours: 35-22-13-9-4.5%

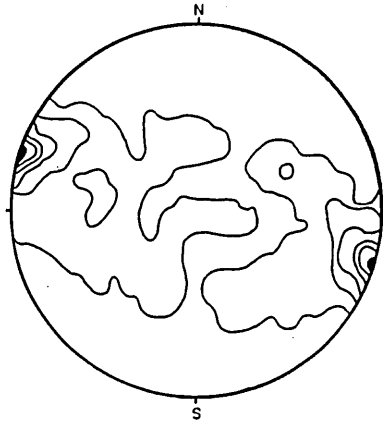


FIG. 21 a)  $\beta$ -diagram for  $S_{1-2}$  of schistose hornfels in subarea C Contours: 40-30-20-10-3-1/2.5%

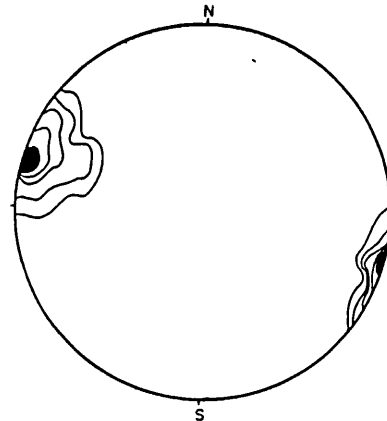


FIG. 21 b)  $L_{2-3}$  of schistose hornfels in subarea C Contours: 40-30-20-10-6.5%

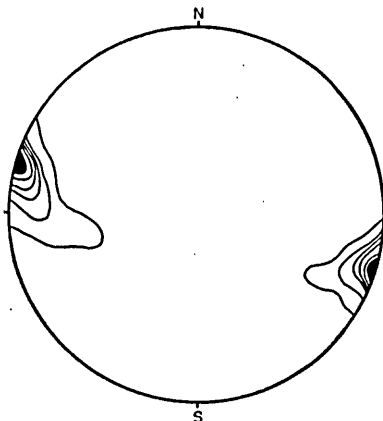


FIG. 22 a)  $\beta$ -diagram for  $S_{1-2}$  of schistose hornfels in subarea D Contours: 50-38-28-12-3-0.421%

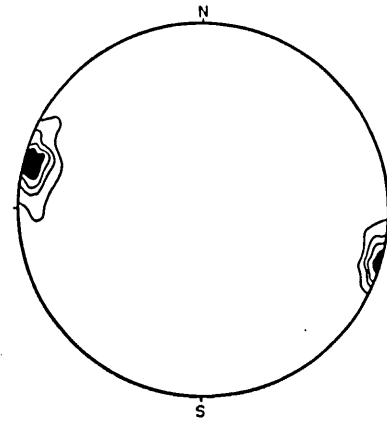


FIG. 22 b)  $L_{2-3}$  of schistose hornfels in subarea D Contours: 35-20-10-5%

map, which corresponds to his Wazuka anticline. If the large anticlinal fold of banded chert near Mt. Oyake is present in fact, it must be inferred that the  $S_{1-2}$ -surfaces in subarea C were produced as slaty cleavage subparallel to the axial surface of the large-scale fold of the banded chert, on the basis of consideration about the structure of the  $S_{1-2}$ -surfaces in subareas A to D mentioned in preceding pages. However, at the boundaries between the banded chert and the pelitic and semi-pelitic rocks in subareas A and B, the  $S_{1-2}$ -surfaces run commonly parallel to them. Unlike subareas A and B, where the banded chert develops fairly abundantly, in subareas C and D the pelitic and semi-pelitic rocks are predominant. Accordingly in places scarcely influenced by movement of neighbouring competent beds, it may be concluded that during the Tamba deformation the  $S_{1-2}$ -surfaces ( $S'_1$ - and  $S''_1$ -surfaces) in the incompetent rocks tended to develop rather parallel to the axial surface of the large-scale fold of competent beds (and probably perpendicular to the maximum compression).

#### B. THE STRUCTURE RELATED TO THE DEFORMATION DURING THE RYOKE METAMORPHIC PHASE

The trends of  $L_{2-3}$ ,  $L_5$ ,  $B_3$ -fold and  $B_5$ -fold in subareas E to K are variable, unlike those in subareas A to D. However, they are not distributed at random.

Subarea E consists mainly of metamorphic derivatives from the pelitic and semi-pelitic rocks. Data for Fig. 23-a and b were measured from those rocks. Fig. 23-a is the  $\pi$ -diagram for  $S_{1-2}$  in subarea E. Poles of  $S_{1-2}$  ( $\pi$ - $S_{1-2}$ ) form a single incomplete girdle on a great circle, containing a marked maximum. The presence of a single marked maximum shows the constancy in the trend of  $S_{1-2}$ , that is the strike  $N64^\circ W$  and the dip  $53^\circ$  to SSW, though in many places the  $S_{1-2}$ -surfaces are folded on small-scale.

The pole of the great circle girdle ( $\pi$ -axis) in Fig. 23-a is clearly to be determined on the diagram. Therefore, it is concluded that, on macroscopic scale, the structure of the  $S_{1-2}$ -surfaces in subarea E shows monoclinic symmetry with a single symmetry plane normal to the  $\pi$ -axis. The azimuth and plunge of the  $\pi$ -axis are  $N64^\circ W$  and  $0^\circ$  respectively.  $L_{2-3}$ -lineations measured in subarea E have been plotted in Fig. 23-b, showing a marked maximum. The azimuth and plunge of the maximum are  $N64^\circ W$  and  $0^\circ$  respectively. The trend of  $L_{2-3}$  coincides with that of the  $\pi$ -axis for  $S_{1-2}$ . Accordingly, the structure of the  $S_{1-2}$ -surfaces in subarea E can safely be ascribed to the deformation related to the formation of  $L_{2-3}$  during the Ryoke metamorphic phase, and furthermore, it is safely concluded that the deformation related to the formation of  $L_5$  and  $B_5$ -folds was not so strong as to give the structure of the  $S_{1-2}$ -surfaces in subarea E a remarkable triclinicity.

In subarea F, most of exposures are of metamorphic derivatives from banded chert. Data for Fig. 24-a and b have been measured from those exposures. In the western part of subarea F the trend of  $L_{2-3}$  shows WNW-ESE, but in the eastern part it changes gradually to SSE. Also the trend of the  $S_{1-2}$ -surfaces changes in close connection with the variation in the trend of  $L_{2-3}$  mentioned above. In the

eastern part of subarea F, anticlinal and synclinal structures of the  $S_{1-2}$ -surfaces having the fold-axes gently plunging towards SSE occur on moderate-scale, as read from the geological map. In the axial zones of those moderate-scale folds, the axial surfaces of the  $B_1$ -folds cut by the  $S_{1-2}$ -surfaces show approximately flat-lying attitude. While, the axial surfaces of the moderate-scale folds in question are dipping at high angles. Therefore, it seems probable that the movement which produced the moderate-scale anticlinal and synclinal structures in the eastern part of subarea F was not that responsible for the formation of the  $B_1$ -folds, that is, the Tamba deformation.

Fig. 24-a is the  $\pi$ -diagram for  $S_{1-2}$  in subarea F. The orientation pattern of  $\pi$ - $S_{1-2}$  is decidedly triclinic. Diagram for  $L_{3-3}$  shows a maximum with considerable spreading (Fig. 24-b). The meaning of those diagrams will be discussed in later pages.

In subarea I, most of exposures are of metamorphic derivatives from banded chert. Data for Fig. 27-a and b have been measured from those exposures.

In the western part of subarea I the  $S_{1-2}$ -surfaces are generally steeply dipping, but in the eastern part they form moderate-scale anticlinal and synclinal structures having the fold-axes gently plunging towards SSE, as read from the geological map. In the axial zones of those moderate-scale folds having their axial surfaces dipping at high angles, those surfaces of the  $B_1$ -folds cut by the  $S_{1-2}$ -surfaces show approximately flat-lying attitude.

The  $\pi$ -diagram for  $S_{1-2}$  in subarea I is shown in Fig. 27-a. Poles of  $S_{1-2}$  ( $\pi$ - $S_{1-2}$ ) form a single complete girdle with maximum and submaxima on a great circle, reflecting the moderate-scale folds mentioned above. The pole of the great circle girdle ( $\pi$ -axis) is clearly to be determined on the diagram, that representing the constant trend of the axes of those folds. Thus, it is safely concluded, on macroscopic scale, the structure of the  $S_{1-2}$ -surfaces in subarea I shows monoclinic symmetry with a single symmetry plane normal to the  $\pi$ -axis. The azimuth and plunge of the  $\pi$ -axis are  $S28^\circ E$  and  $34^\circ$  respectively.  $L_{2-3}$ -lineations in subarea I have been plotted in Fig. 27-b, which shows a marked maximum. The azimuth and plunge of the maximum are approximately  $S30^\circ E$  and  $34^\circ$  respectively. The trend of  $L_{2-3}$  coincides with that of the  $\pi$ -axis for  $S_{1-2}$ . Accordingly, the structure of the  $S_{1-2}$ -surfaces in subarea I can be correlated with the deformation related to the formation of  $L_{2-3}$  during the Ryoike metamorphic phase, as is the case for subarea E, though the  $\pi$ -axis for  $S_{1-2}$  in both subareas show quite different trend. In this case it is also shown that the deformation related to  $L_5$  and  $B_5$ -folds is not so strong as to give the structure of the  $S_{1-2}$ -surfaces in subarea I a remarkable triclinicity, as is the case for subarea E.

Subarea H consists mainly of metamorphic derivatives from the pelitic and semipelitic rocks. Data for Fig. 26-a and b have been measured from those rocks.

The  $S_{1-2}$ -surfaces in subarea H form anticlinal and synclinal structures corresponding to those in subareas F and I described in preceding pages. The  $\pi$ -diagram for

$S_{1-2}$  in subarea H is shown in Fig. 26-a. Apparently, this diagram does not represent the distribution of  $\pi$ - $S_{1-2}$  corresponding to the anticlinal and synclinal structures mentioned above. It is due to the reason that most of exposures in subarea H, from which the data in question were measured, are situated along the river Uchitaki running approximately parallel to the direction of strike of the  $S_{1-2}$ -surfaces.  $\pi$ - $S_{1-2}$  forms a distinct great circle girdle. The  $\pi$ -axis for the great circle girdle can be clearly determined on the diagram. The azimuth and plunge of the  $\pi$ -axis are  $S28^\circ E$  and  $34^\circ$  respectively, showing the same trend as that in subarea I.  $L_{2-3}$ -lineations measured in subarea H have been plotted in Fig. 26-b, which shows a marked maximum with considerable spreading. The azimuth and plunge of the maximum are  $S29^\circ E$  and  $34^\circ$  respectively. The trend of  $L_{2-3}$  coincides with that of the  $\pi$ -axis for  $S_{1-2}$ , that giving the same conclusions as for subareas E and I mentioned in preceding pages with respect to the geometry of the structure of  $S_{1-2}$ -surfaces.

Subarea F is situated at the jointing position between subareas E and H. In the  $\pi$ -diagram for  $S_{1-2}$  of Fig. 24-a, it can be pointed out that the  $\pi$ -circle<sub>1</sub> corresponds approximately to the attitude of  $S_{1-2}$ -surfaces in the western part of subarea F, on the basis of careful examination about the distribution of  $\pi$ - $S_{1-2}$  measured from this partial area. The pole of  $\pi$ -circle<sub>1</sub> ( $\pi$ -axis<sub>1</sub>) has the azimuth and plunge of  $S65^\circ E$  and  $11^\circ$  respectively. The direction of  $\pi$ -axis<sub>1</sub> is very close to that of the  $\pi$ -axis for  $S_{1-2}$  in subarea E shown in Fig. 23-a. While, in Fig. 24-a, the  $\pi$ -circle<sub>2</sub> reflects the moderate-scale anticlinal and synclinal structures of the  $S_{1-2}$ -surfaces in the eastern part of subarea F. The pole of  $\pi$ -circle<sub>2</sub> ( $\pi$ -axis<sub>2</sub>) has the azimuth and plunge of  $S25^\circ E$  and  $35^\circ$  respectively, the direction being very close to that of the  $\pi$ -axis for  $S_{1-2}$  in subareas H and I examined in preceding pages. Passing from the west to the east in subarea F, the trends of the  $S_{1-2}$ -surfaces and  $L_{2-3}$ -lineations change gradually. The orientation patterns of  $\pi$ - $S_{1-2}$  and  $L_{2-3}$  in Fig. 24-a and b reflect this fact. It is pointed out that within subareas E, F, H and I the change in the trends of the  $L_{2-3}$ -lineations and of the fold statistically defined by the distribution of  $\pi$ - $S_{1-2}$  represents a remarkable arcuation, the trend changing from ESE to SSE.

Subarea G consists mainly of metamorphic derivatives from the pelitic and semi-pelitic rocks. Data for Fig. 25-a and b were obtained from those rocks. Fig. 25-a is the  $\pi$ -diagram for  $S_{1-2}$ .  $\pi$ - $S_{1-2}$  forms a single incomplete girdle on a great circle. The  $\pi$ -axis for the great circle girdle can be clearly determined on the diagram, that indicating the monoclinic symmetry of the structure in subarea G, that is, statistically homogeneous with respect to the  $\beta$ -axis. The azimuth and plunge of the  $\pi$ -axis are  $N30^\circ E$  and  $57^\circ$  respectively.  $L_{2-3}$ -lineations have been plotted in Fig. 25-b, showing a maximum with considerable spreading on a great circle. The trend of the maximum does not coincide with that of the  $\pi$ -axis, but the former is perpendicular to the latter, unlike the relation observed in subareas E, F, H and I. The great circle, in which  $L_{2-3}$ -lineations spread, coincides with the  $\pi$ -circle for  $S_{1-2}$ . In many places of subarea G, are found the  $B_6$ -folds, which destroyed by the super-

position the high symmetry of the structure of  $S_{1-2}$ -surfaces, generally, a monoclinic symmetry with a single symmetry plane normal to  $L_{2-3}$ . The orientation of the  $B_6$ -folds is shown by solid circles in Fig. 25-b. The azimuth and plunge of the average trend of  $B_6$ -folds are  $N35^\circ E$  and  $57^\circ$  respectively, coinciding approximately with the trend of the  $\pi$ -axis in Fig. 25-a. Therefore, it may be concluded that the structure of  $S_{1-2}$ -surfaces, which had been monoclinic with reference to  $L_{2-3}$ , was reconstructed by the deformation related to the formation of the  $B_6$ -folds.

The  $B_6$ -folds have been observed also in many places of subarea H. The axes of  $B_6$ -folds are concentrated within a small area in Fig. 26-c. The center of the distribution area shows approximately the plunge of  $58^\circ$  towards N. In Fig. 23-a is to be traced the distribution of  $\pi$ - $S_{1-2}$  along the zone about the axes of  $B_6$ -folds, though it is weak.

Also in subareas F and I, the  $B_6$ -folds and  $L_6$ -lineations have been sporadically observed.

In subarea J, most of exposures are of metamorphic derivatives from banded chert. Data for Figs. 28-a and b were obtained from those exposures.

In the northern part of subarea J, the trend of  $L_{2-3}$  shows SSE, but towards the southern part it changes gradually to SSW. The  $S_{1-2}$ -surfaces form moderate-scale anticlinal and synclinal structures corresponding to those in subarea I, as read from the geological map. Also the trend of the moderate-scale folds changes in close connection with the variation in the trend of  $L_{2-3}$ , showing a weak arcuation. This relation with respect to the trend of  $S_{1-2}$  and  $L_{2-3}$  is clearly represented in the orientation pattern of  $\pi$ - $S_{1-2}$  and  $L_{2-3}$  in Fig. 28-a and b.

In the  $\pi$ -diagram for  $S_{1-2}$  of Fig. 28-a, it can be pointed out that the  $\pi$ -circle<sub>1</sub> corresponds approximately to the attitude of  $S_{1-2}$  in the northern part of subarea J, on the basis of examination of the distribution of  $\pi$ - $S_{1-2}$  measured from this partial area. The azimuth and plunge of the pole of  $\pi$ -circle<sub>1</sub> ( $\pi$ -axis<sub>1</sub>) are  $S34^\circ E$  and  $20^\circ$  respectively, the direction coinciding approximately with the trend of  $L_{2-3}$  in the same partial area. While,  $\pi$ -circle<sub>2</sub> corresponds approximately to the attitude of  $S_{1-2}$  in the southern area. The azimuth and plunge of the pole of  $\pi$ -circle<sub>2</sub> ( $\pi$ -axis<sub>2</sub>) are  $S31^\circ W$  and  $22^\circ$  respectively, the direction coinciding approximately with the trend of  $L_{2-3}$  in the same partial area. The orientation pattern of  $L_{2-3}$  in Fig. 28-b is characterized by an incomplete great circle girdle with a maximum. The presence of maximum seems to be due to the reason that many of exposures, from which  $L_{2-3}$ -lineations were measured, are distributed in the northern half of subarea J. The pole of the great circle girdle has the azimuth and plunge of  $N3^\circ E$  and  $65^\circ$  respectively. The point of intersection of the  $\pi$ -circle<sub>1</sub> and  $\pi$ -circle<sub>2</sub> (here termed  $B_6$ -axis) shows the azimuth and plunge of  $N12^\circ E$  and  $67^\circ$  respectively. The pole of the great circle girdle for  $L_{2-3}$  coincides approximately with the trend of  $B_6$ -axis. Thus, the  $B_6$ -axis corresponds to the rotational axis with respect to the variation (arcuation) in the trend of  $L_{2-3}$  and the moderate-scale folds in subarea J mentioned above.

In many places of subarea J, the  $B_6$ -folds and  $L_6$ -lineations are observed. They

have been collectively plotted in Fig. 28-c, in which a marked maximum is shown. The azimuth and plunge of the maximum are N20°E and 68° respectively. The trend of B<sub>6</sub>-folds and L<sub>6</sub> coincides approximately with that of B<sub>6</sub>-axis in Fig. 28-a. Accordingly, the formation of the arcuation in subarea J can be ascribed to the deformation related to the formation of B<sub>6</sub>-folds and L<sub>6</sub>.

Metamorphic rocks in subarea K develop as xenolithic masses in the Sakawa granodioritic rocks in the western part of the district. They consist mainly of derivatives from banded chert.

The S<sub>1-2</sub>-surfaces in subarea K tend to dip at high angles towards WSW~SW, as a whole, though they are generally remarkably folded on small scale. Fig. 29-a is the  $\pi$ -diagram for S<sub>1-2</sub>. The diagram is characterized by the presence of two great circle girdles and two maxima: the one is a complete girdle with one maximum ( $\pi$ -circle<sub>1</sub>) and the other is an incomplete girdle with two maxima ( $\pi$ -circle<sub>2</sub>). From careful examination about the distribution of localities, where  $\pi$ -S<sub>1-2</sub>, which forms the dotted part of  $\pi$ -circle<sub>1</sub> in Fig. 29-a, was measured,  $\pi$ -circle<sub>1</sub> seems to correspond not to the general trend of the S<sub>1-2</sub>-surfaces in subarea K, but to a moderate-scale fold of S<sub>1-2</sub> in an exposure northeast of Sakawahigashi. In other exposures in subarea K, such moderate-scale fold has not been found, and the  $\pi$ -diagram reflects this fact. As mentioned above, the S<sub>1-2</sub>-surfaces in subarea K tend to dip at high angles towards WSW~SW, as a whole.

The pole of  $\pi$ -circle<sub>2</sub> ( $\pi$ -axis<sub>2</sub>) has the azimuth and plunge of S15°W and 67° respectively. In some places of subarea K, the B<sub>6</sub>-folds have been found (Fig. 29-c). The azimuth and plunge of the average trend of them are S36°W and 68° respectively, the direction coinciding approximately with the trend of  $\pi$ -axis<sub>2</sub> in Fig. 29-a. This relation seems not to be dissimilar to that of those structural elements in subarea G. The orientation pattern of L<sub>2-3</sub>-lineations is illustrated in Fig. 29-b. Some of them have steep plunge of ca. 60°. While, the trend of the B<sub>6</sub>-folds is approximately constant all over subarea K as shown in Fig. 29-c. Therefore, it may safely be concluded that remarkable variation in plunge of L<sub>2-3</sub> within subarea K had existed prior to the deformation related to the formation of the B<sub>6</sub>-folds. As will be discussed in later pages, the variation in plunge of L<sub>2-3</sub> seems to be due to the reason that some bodies of metamorphic rocks in subarea K were displaced by the intrusion of the Sakawa granodioritic rocks.

The pole of  $\pi$ -circle<sub>1</sub> ( $\pi$ -axis<sub>1</sub>), that is, the axis of the moderate-scale fold of S<sub>1-2</sub> in an exposure northeast of Sakawahigashi mentioned above, coincides approximately with the trend of L<sub>2-3</sub> in the same exposure. The change in the trend of S<sub>1-2</sub> within subarea K shown by the  $\pi$ -circle<sub>2</sub> in Fig. 29-a is accompanied by the corresponding change in the trend of L<sub>2-3</sub>, that being quite similar to the geometrical relation between them in subareas F, G, and J described in preceding pages.

For reference purpose, lastly, will be described geometrical relation between the S<sub>1-2</sub>-surface, L<sub>2-3</sub>-lineation, B<sub>6</sub>-fold and L<sub>6</sub>-lineation of the metamorphic rocks in the area between Mima and Goe of a few kilometers beyond the southern limit of the

mapped area. Metamorphic rocks in this area consist of derivatives from pelitic rock, sandstone, banded chert and basic igneous rocks.

The  $S_{1-2}$ -surfaces in the area in question tend to dip at high angles towards N~NNE as a whole. Fig. 30-a is the  $\pi$ -diagram for  $S_{1-2}$ .  $\pi$ - $S_{1-2}$  forms a single incomplete girdle on a great circle. The  $\pi$ -axis of the great circle girdle can be determined on the diagram, that indicating the monoclinic symmetry of the structure of  $S_{1-2}$ -surface on macroscopic scale. The  $\pi$ -axis shows plunge of  $56^\circ$  towards N.  $L_{2-3}$ -lineations have been plotted in Fig. 39-b, showing a maximum with respectable spreading. The trend of the maximum does not coincide with that of the  $\pi$ -axis, but the former is perpendicular to the latter, just like the relation observed in sub-area G. In many places of the area in question are found the  $B_6$ -folds and  $L_6$ -lineations. The orientation of them is illustrated in Fig. 30-b. They show average plunge of  $55^\circ$  towards  $N7^\circ E$ , the direction coinciding approximately with the trend of the  $\pi$ -axis in Fig. 30-a. Therefore, it may be concluded that the structure of  $S_{1-2}$ -surface, which had been monoclinic with reference to  $L_{2-3}$ , was reconstructed by the deformation related to the formation of the  $B_6$ -folds and  $L_6$ -lineations. The area in question is designated as subarea L for convenience sake through following discussions.

The trend of  $L_{2-3}$  and the  $\beta$ -axis for  $S_{1-2}$  in subareas C and D, where the structures is homogeneous with respect to those elements, coincides approximately with that of the Ryoke zone in Kinki Province. While, in subareas F to K, the trend of those structural elements makes appreciable angles with the trend of the Ryoke zone, that suggesting the presence of a large-scale cross-fold in the district.

Recently the presence of cross-folds in mountain chains has been reported by many worker, and the theories of their origin have been discussed with reference to many examples. They can be divided into two groups. According to RAST and PLATT (1957), 1) "some suggest that each individual trend of folding indicates an independent orogeny or at least an orogenic episode..." and 2) "others (e.g. ENGEL 1949, KING 1955, CROSS 1955) have suggested that, at least in metamorphic rocks of geosynclinal belts, the main and the cross-fold trends are essentially simultaneous. Alpine geologists recognized this possibility long ago."

Judging from geometrical relations of  $L_{2-3}$ , the  $\beta$ -axis for  $S_{1-2}$ , the  $B_6$ -folds and  $L_6$  in subareas F to L, with respect to the formation of the large-scale cross-fold in the district, the first theory seems to be valid for the presence. The problems, why the  $B_6$ -folds and  $L_6$ -lineations, which destroyed the structure of  $S_{1-2}$ -surfaces with high symmetry with respect to  $L_{2-3}$ , have geometrically quite harmonic connection with the cross-fold in question and also why, in spite of remarkable variation in plunge of  $L_{2-3}$ , subarea K is homogeneous with respect to the  $\pi$ -axis, seem to be more clearly illustrated by application of the first theory about the origin of cross-fold in the district than by that of the second theory. Therefore, it may be concluded that the trend of the cross-fold in the district was determined by the displacement of the structure of  $S_{1-2}$ -surfaces with  $L_{2-3}$  and the  $\beta$ -axis for  $S_{1-2}$  trending to WNW-

ESE by the deformation related to the formation of the  $B_6$ -folds and  $L_6$ . Some doubts remains, however, since, even in subareas F to K corresponding to a limb of the cross-fold in question, the  $B_6$ -fold and  $L_6$ -lineation are only weakly developed.

$L_{2-3}$ -lineations of metamorphic rocks and lineations of the Sakawa granodioritic rocks plunge towards ESE~SSE at the eastern side of the line connecting Sakawahigashi, through Hirooka, to the east of Kiriyaama, while they plunge towards WNW~NNW at the western side of the line, as a whole. This fact suggests that there is an anticline on large-scale, the axis of which coincides with the line connecting Sakawahigashi to the east of Kiriyaama with reference to its azimuth. This anticlinal structure represents the youngest structure in the district, which were formed after the Ryoke metamorphism ceased.

With this fact in mind, the geometry of the movement related to the  $B_6$ -folds and  $L_6$  will be examined on the basis of considerations about the regional preferred orientation of structural elements described in preceding pages. The  $B_6$ -folds and  $L_6$ -lineations tend to run commonly approximately perpendicularly to  $L_{2-3}$ , except in some places of subarea K. The trend of the  $B_6$ -folds and  $L_6$  depends upon the strike and dip of  $S_{1-2}$ -surfaces concerned, as clearly shown in the geometrical relation between them in subareas G, K and L. They have been mainly observed on the  $S_{1-2}$ -surfaces dipping at angles of between  $40^\circ$  and  $90^\circ$ .

Where the  $S_{1-2}$ -surfaces dip homoclinally at high angles as a whole, the symmetry of strain in the deformation related to the formation of the  $B_6$ -folds and  $L_6$  (cross-folding on large-scale) was monoclinic and the deformation plane must have been a plane normal to the  $B_6$ -fold and  $L_6$ , as clearly represented in geometrical relations of  $S_{1-2}$ ,  $L_{2-3}$ ,  $B_6$ -fold and  $L_6$  in subareas G, K and L. Though the  $B_6$ -folds and  $L_6$  show different azimuth between subareas G, K and L respectively, where the  $S_{1-2}$ -surfaces dip at similar angle to each other, their plunges show similar value through those subareas. The  $B_6$ -folds and  $L_6$  measured from those subareas have been collectively plotted in Fig. 31. The diagram is characterized by an incomplete girdle on a small circle with angular radius of ca.  $25^\circ$ . The center of the small circle girdle coincides with that of the diagram, the direction being vertical with reference to the geographical coordinates. Accordingly it may be concluded that, as a whole, the district experienced a deformation with the axis of external rotation vertically plunging with reference to the geographical coordinates, though within each of small fields of the district the deformation had taken place with respect to the  $b$ -kinematic axis coinciding with the  $B_6$ -folds and  $L_6$  (their trends depending upon the trend of  $S_{1-2}$ -surfaces). This conclusion is not in contradiction to the geometrical relations of  $S_{1-2}$ ,  $L_{2-3}$ ,  $B_6$ -fold and  $L_6$  in subareas F, H and J.

While, deformation style of flat-lying  $S_{1-2}$ -surfaces in the axial zones of the moderate-scale folds having their axis parallel to  $L_{2-3}$  is not obvious, development of the  $B_6$ -folds and  $L_6$  being quite insignificant. Subarea I is a monoclinic field statistically homogeneous with respect to the  $\beta$ -axis, which trends parallel to  $L_{2-3}$ . These facts seem to suggest that, during the deformation in question, in the axial zones of the

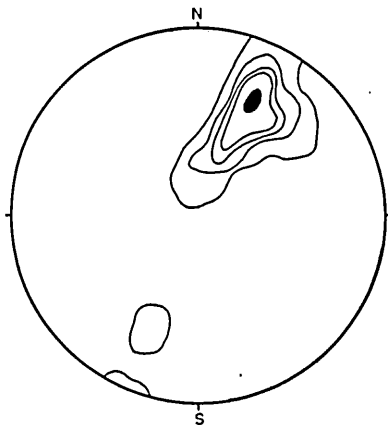


FIG. 23 a)  $\pi$ -diagram for  $S_{1-2}$  of schistose hornfels and gneisses in subarea E. Contours: 18-14-10-6-1%

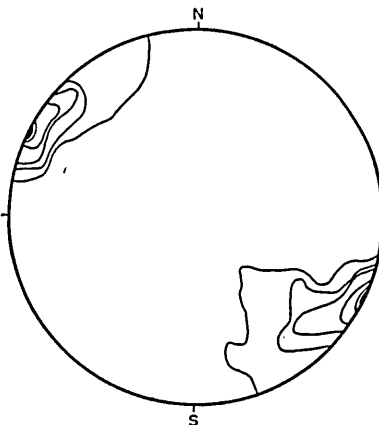


FIG. 23 b)  $L_{2-3}$  of schistose hornfels and gneisses in subarea E. Contours: 12-10-8-5-3-1%

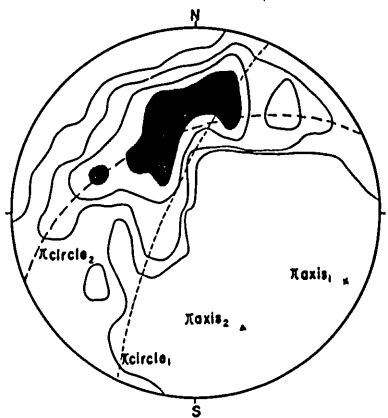


FIG. 24 a)  $\pi$ -diagram for  $S_{1-2}$  of schistose hornfels and gneisses in subarea F. Contours: 10-5-3-1%

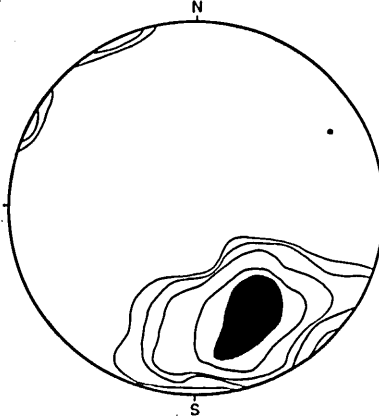


FIG. 24 b)  $L_{2-3}$  of schistose hornfels and gneisses in subarea F. Contours: 15-10-5-3-1%

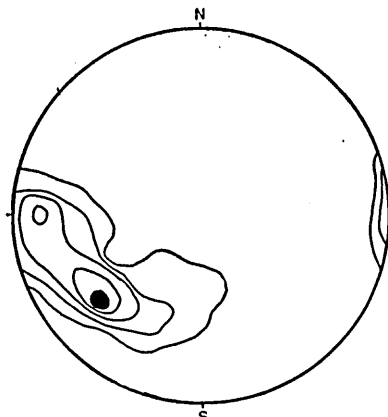


FIG. 25 a)  $\pi$ -diagram for  $S_{1-2}$  of schistose hornfels in subarea G. Contours: 10-7-5-3-1%

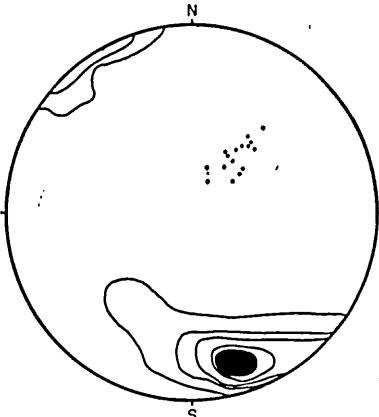


FIG. 25 b)  $L_{2-3}$  of schistose hornfels in subarea G (density diagram) and axes of the  $B_0$ -folds and  $L_0$  in subarea G (scatter diagram) Contours: 10-7-5-3-1%

Studies on the Structure of the Ryoke Metamorphic Rocks of the Kasagi District, Southwest Japan

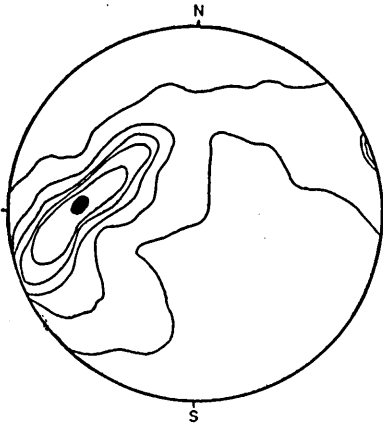


FIG. 26 a)  $\pi$ -diagram for  $S_{1-2}$  of schistose hornfels and gneisses in subarea H. Contours: 13-10-7-5-3-0.5%

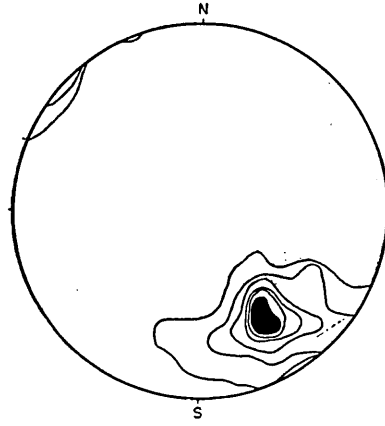


FIG. 26 b)  $L_{2-3}$  of schistose hornfels and gneisses in subarea H. Contours: 20-15-10-6-3-1%

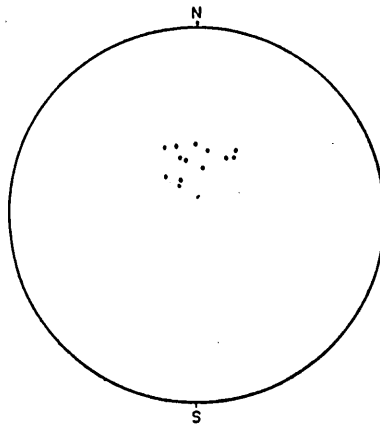


FIG. 26 c) Axes of the  $B_6$ -folds and  $L_6$  of schistose hornfels and gneisses in subarea H

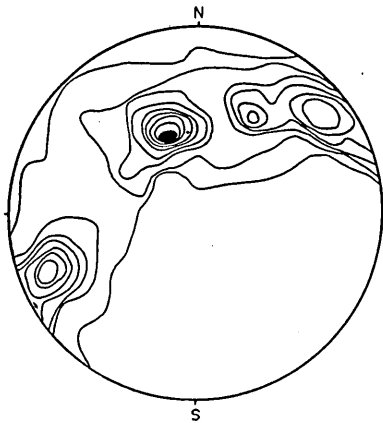


FIG. 27 a)  $\pi$ -diagram for  $S_{1-2}$  of schistose hornfels and gneisses in subarea I. Contours: 20-15-13-11-9-7-5-3-1%

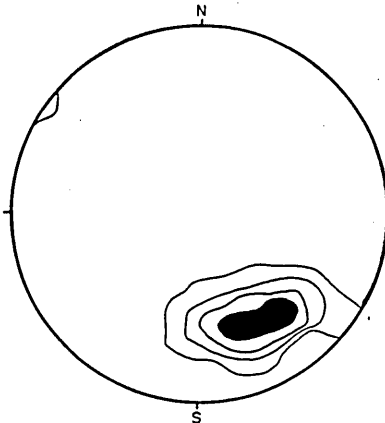


FIG. 27 b)  $L_{2-3}$  of schistose hornfels and gneisses in subarea I. Contours: 20-10-5-1%

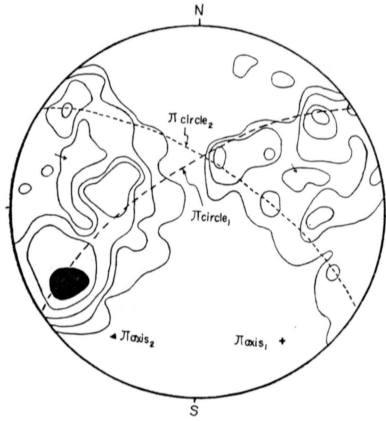


FIG. 28 a)  $\pi$ -diagram for  $S_{1-2}$  of gneisses in subarea J. Contours: 13-6-3-2-1%

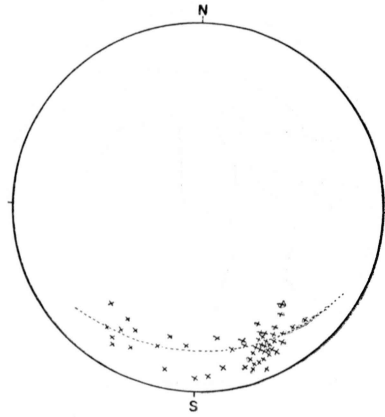


FIG. 28 b)  $L_{2-3}$  of gneisses in subarea J.

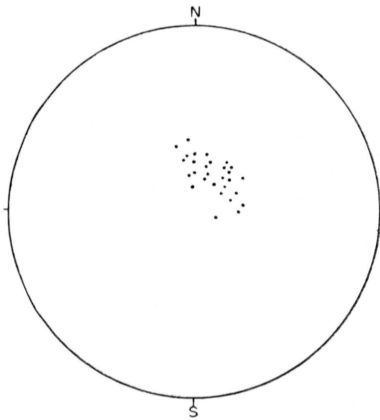


FIG. 28 c) Axes of the  $B_0$ -folds and  $L_6$  of gneisses in subarea J.

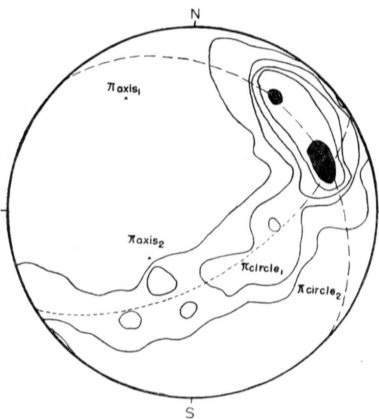


FIG. 29 a)  $\pi$ -diagram for  $S_{1-2}$  of gneisses in subarea K. Contours: 10-7-5-3-1%

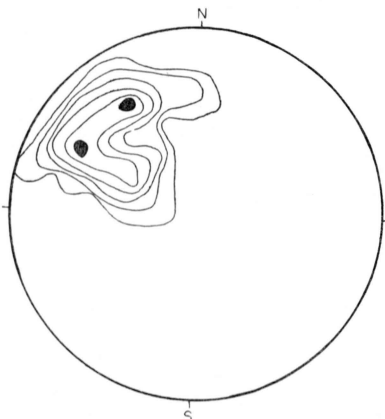


FIG. 29 b)  $L_{2-3}$  of gneisses in subarea K. Contours: 10-8-6-4-2-1%

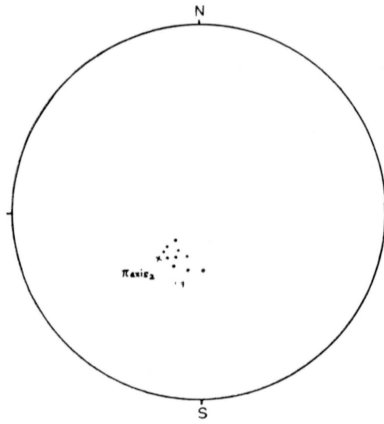


FIG. 29 c) Axes of the  $B_6$ -folds and  $L_6$  of gneisses in subarea K.

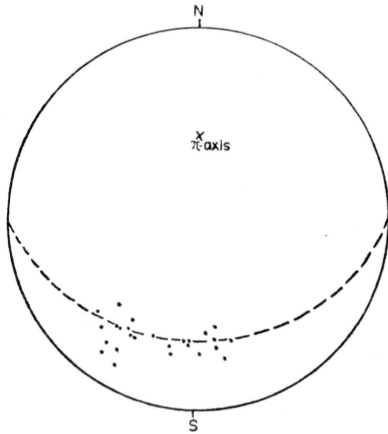


FIG. 30 a)  $\pi$ -diagram for  $S_{1-2}$  of gneisses in subarea L.

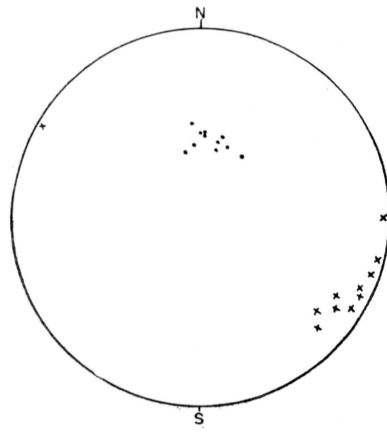


FIG. 30 b)  $L_{2-3}$  of gneisses in subarea L (cross) and axes of the  $B_6$ -folds and  $L_6$  in subarea L (dot).

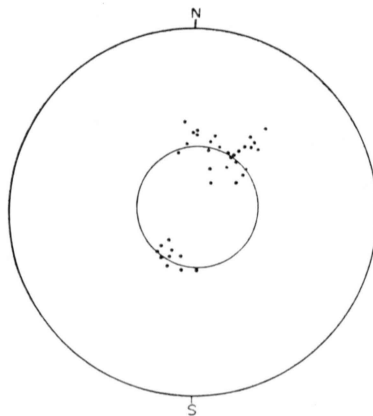


FIG. 31 Synoptic diagram of Figs. 25-b, 29-c and 30-b.

moderate-scale folds shear movement along  $S_{1-2}$ -surfaces was inactive. The mica- and quartz-fabrics, which will be discussed in detail in the chapter V, give favourable data for this interpretation.

On the basis of preceding descriptions and discussions, tectonic sequence during the Ryoke metamorphic phase can be divided into two main stages: 1) the older Ryoke deformation having the  $b$ -kinematic axis gently plunging towards WNW-ESE, and 2) the younger Ryoke deformation in which the structure which had been produced by the older Ryoke deformation was refolded with respect to the axis of external rotation vertically plunging with reference to the geographical coordinates as a whole, accompanied with the formation of the  $B_6$ -folds and  $L_6$ -lineations corresponding to the  $b$ -kinematic axis within each of small fields of the district.

The  $B_5$ -folds and  $S_5$  are older than the  $B_6$ -folds and  $L_6$ , and generally trend sub-parallel to  $L_{2-3}$ . Accordingly, the stage of the older Ryoke deformation can be further divided into two substages with reference to those structural elements: 1)  $B_3$ -substage, corresponding to the formation of the  $B_3$ -folds and  $L_{2-3}$ , and 3)  $B_5$ -substage, corresponding to the formation of the  $B_5$ -folds,  $S_5$ -surfaces and  $L'_5$ .

It seems probable that the  $S_{1-2}$ -surfaces in subareas C and D inclined homoclinally at high angles towards NNE before the older Ryoke deformation took place, judging from the conclusion about incipient attitude of  $S_{1-2}$ -surfaces in those subareas. The present folded structure of  $S_{1-3}$  in those subareas shows a monoclinic symmetry with a single symmetry plane normal to  $L_{2-3}$ . The symmetry of movement in each substage of the older Ryoke deformation was rather monoclinic, and the deformation plane must have had a NNE-SSW strike and approximately vertical dip. Judging from the present attitude of the  $S_{1-2}$ -surfaces in subareas C and D when compared with incipient attitude of  $S_{1-2}$ , the direction of movement in the older Ryoke deformation seems to have been NNE as a whole. The geometrical relation between the  $\beta$ -axis for  $S_{1-2}$  and  $L_{2-3}$  in subarea A, however, represents that the older Ryoke deformation was insignificant in this subarea. Therefore, it may be concluded that it became suddenly weak, passing from subarea D to the north.

## V. MICROSCOPIC STRUCTURES

### A. MICROSCOPIC CONJUGATE TRANSVERSAL SURFACES PARALLEL TO $L_{2-3}$

Prior to descriptions and discussions of microscopic structures of the rocks concerned, the principal fabric axes will be set up conveniently in accordance with the principal schistosity  $S_{1-2}$  and the principal lincation  $L_{2-3}$ , *i.e.*, the axis  $b$  coincides with the direction of the principal lincation  $L_{2-3}$ , the axis  $a$  is perpendicular to  $L_{2-3}$  on the  $S_{1-2}$ -surfaces, and the axis  $c$  is normal to the  $S_{1-2}$ -surface.

In thin sections normal to  $L_{2-3}$  for metamorphic derivatives from the pelitic and semi-pelitic rocks collected from many places of subareas C and D, microscopic planar structural surfaces which traverse  $S_{1-2}$  have been recognized. They are represented by parallel sets of slip zones as shown in Plate 1-2 and 2. In those slip

zones, flakes of micas are bent completely or incompletely to the direction of them. The direction of relative movement in the slip zone can be established on the basis of careful examination about rotated flakes of micas in the slip zone, as discussed by E. INGERSON (1936) with reference to muscovite-biotite-schist from Niederthal, Tyrol.

Generally, the line of intersection of the  $S_{1-2}$ -surfaces and the transversal surfaces in question coincides strictly with the direction of  $L_{2-3}$ . In some places, the transversal surfaces are displayed as two sets which are almost symmetrically oriented to  $S_{1-2}$ . The sense of slip movement on them is reversed between these two sets. This kinematic relation suggests that these two sets of transversal surfaces correspond to a pair of shear surfaces formed by the deformation of the type of two dimensional flattening, and  $L_{2-3}$  coincides with a single symmetry axis of this deformation. These two sets of transversal surfaces are designated as  $S_3$  and  $S_4$  respectively.

In many places, however, only either one set of them develops, probably reflecting the influence of external rotation overlapped on the flattening.

Also in some places of subarea B, the transversal surfaces  $S_3$  and  $S_4$  have been observed in the pelitic and semi-pelitic rocks.

In metamorphic derivatives (chiefly gneiss) from the pelitic and semi-pelitic rocks in subareas E to K, microscopic structural surfaces parallel to  $L_{2-3}$  which traverse  $S_{1-2}$  have been sporadically observed. They are represented by parallel arrangement of flakes of micas, being usually developed in one set (Plate 19-3).

In most of orientation diagrams for  $[001]$  of micas in metamorphic derivatives from banded chert in subareas E to K, submaxima on the  $ac$  great circle, which do not correspond to  $S_{1-2}$ , are found, as will be examined in later pages. Those submaxima seem to represent the presence of parallel surfaces, which traverse  $S_{1-2}$  and are tautozonally oriented with respect to  $L_{2-3}$ . Those statistically inferred surfaces

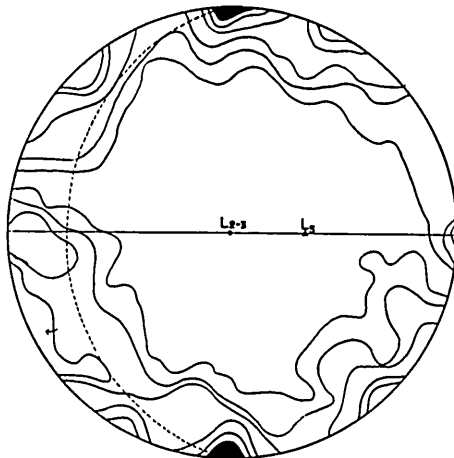


FIG. 32 200  $[001]$  of micas in siliceous schistose hornfels from about 200 m to the east of Hirooka.  
Contours: 7-6-5-3-2-1%

are generally displayed as two sets which are almost symmetrically oriented to  $S_{1-2}$ .

Fig. 32 is the diagram for [001] of micas prepared from thin section normal to  $L_{2-3}$  of a specimen collected from a limb of the  $B_5$ -fold (banded chert from subarea F). A maximum and two submaxima in the diagram are oriented on the  $ac$  great circle. The two submaxima suggest the presence of two sets of transversal surfaces oriented tautozonally with respect to  $L_{2-3}$ . Therefore, it may be concluded that these two sets of transversal surfaces had been formed before the deformation related to the  $B_5$ -folds and  $L_5$  took place. The  $b$ -kinematic axis in the strain for the formation of those surfaces seems to coincide with the direction of  $L_{2-3}$ , judging from the result of analysis of mica and quartz fabrics in later pages.

Strictly speaking, it is not obvious whether those two sets of transversal surfaces correspond to the  $S_3$ - and  $S_4$ -surfaces in subareas B, C and D with reference to the time of the formation of them or not. It is obvious, however, that all those transversal surfaces had been formed throughout the district before the  $B_5$ -substage of deformation. The kinematics with respect to the formation of  $S_3$  and  $S_4$  in subareas B, C and D examined in preceding pages may be valid for the transversal surfaces in metamorphic derivatives from banded chert in subareas E to K described above, judging from the fact that in most cases these surfaces are displayed as two sets which are almost symmetrically oriented to  $S_{1-2}$ . On the basis of these considerations, microscopic transversal surfaces parallel to  $L_{2-3}$  described above are collectively designated as  $S_3$  and  $S_4$  in this paper.

#### B. SIGNIFICANCE OF THE DEFORMATION RELATED TO THE $B_5$ -FOLDS, $L_5$ , AND THE $S_3$ -SURFACES

##### 1. Petrofabric analysis of a $B_3$ -fold

Since B. SANDER (1930) had reported his classic petrofabric studies about small-scale folds of the rocks of various types in Tyrol, detailed petrofabric analyses of folds have been made by many workers. A method of petrofabric analysis of polygenetic fold had been described by J. LADURNER (1954). K. A. JONES (1959) applied this method to the analysis of fold with a complicated tectonic history from the Darladian of western Perthshire, but he came to the conclusion that "the technique gives results allowing a clear cut interpretation only when one strong maximum occurs in the quartz diagram." A  $B_3$ -fold of psammitic gneiss collected from the central part of subarea E has been analysed with reference to the petrofabric method of Ladurner.

The  $B_3$ -fold in question shows monoclinic symmetry with a single symmetry plane normal to the fold-axis. The included angle of limbs of the fold is about  $55^\circ$ . From megascopic observation of the fold in question, it seems to be of the concentric type. In inner axial part (sector F) of knee of the fold, micro-folds shown by polygonal orientation of flakes of micas and fibrolites with an average wave length of ca 0.78 mm develop, suggesting that the fold in question might have been produced by flexure-slipping on  $S_{1-2}$ .

In thin section normal to  $L_{2-3}$ , the shapes of quartz grains are generally rather equidimensional, and they vary in size from 0.02 to 1.3mm. However, any available

relation between the variation in size of quartz grains and their distribution with reference to spatial position on the fold has been not recognized, unlike quartz fold from Brixen Rien Schulucht, South Tyrol, described by I. SCHÄFFLER-ZOZMANN (1955).

The fold in question was divided into six sectors (A, B, C, D, E and F) as shown in Fig. 33. The quartz diagrams have been made in all sectors, and the mica diagrams in sectors A, C and D.

Sector A. The mica diagram (Fig. 35-b) is characterized by a sharply defined *ac* girdle with a maximum and a submaximum. The maximum corresponds strictly to  $S_{1-2}$ , and the submaximum represents the presence of one set of (*hOl*)-surface. The quartz diagram (Fig. 35-a) is characterized by a sharply defined *ac* girdle with a maximum and two submaxima. The maximum and one of the submaxima have no separate significance and can be grouped together as one maximum group, this corresponding to the position of Maximum I after SANDER (1950) with reference to  $S_{1-2}$ . The other submaximum is Maximum I with reference to the (*hOl*)-surface. Angular distance between the maximum group and submaximum is approximately  $55^\circ$ . The rock is a B-tectonite.

Sector C. The mica diagram (Fig. 37-b) is characterized by a sharply defined *ac* girdle with a maximum and a submaximum (low concentration.) The maximum corresponds strictly to  $S_{1-2}$ , and the submaximum may suggest the presence of one set of (*hOl*)-surface. The quartz diagram (Fig. 39-a) is characterized by a complete *ac* girdle with a maximum and a submaximum. The maximum is Maximum I with reference to  $S_{1-2}$ , and the submaximum is Maximum I with reference to the (*hOl*)-surface. Angular distance between the maximum and submaximum is approximately  $70^\circ$ .

Sector E. The mica diagram (Fig. 39-b) is characterized by a sharply defined *ac* girdle with a maximum and a submaximum. The maximum corresponds strictly to  $S_{1-2}$ , and the submaximum may suggest the presence of one set of (*hOl*)-surface. The quartz diagram (Fig. 39-a) is characterized by a complete *ac* girdle with a maximum and two submaxima. The maximum is Maximum I with reference to  $S_{1-2}$ . Two submaxima have no separate significance and can be grouped together as one submaximum group, this corresponding to Maximum I with reference to the (*hOl*)-surface. Angular distance between the maximum and submaximum group is approximately  $64^\circ$ .

Thus, it is pointed out that the mica and quartz fabrics in sectors A, C and E are quite similar to each other, showing a quartz maximum corresponding to Maximum I with reference to  $S_{1-2}$  and a submaximum corresponding to Maximum I with reference to one set of (*hOl*)-surface. Also quartz fabrics in sectors B and D show similar pattern to those in sectors A, C and E described above, as read from Figs. 36 and 38. While, quartz fabric (Fig. 40) in the inner axial area (sector F) of the knee of the fold shows different pattern from that in other sectors. This diagram is characterized by a complete *ac* girdle with a maximum and five submaxima, probably reflecting

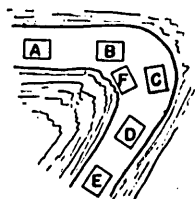


FIG. 33 Diagram of fold showing position of sectors. The sections were cut normal to the fold axis.

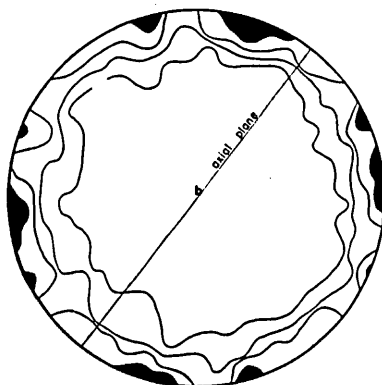


FIG. 34 Collective diagram of the quartz made of the fold in the present form.

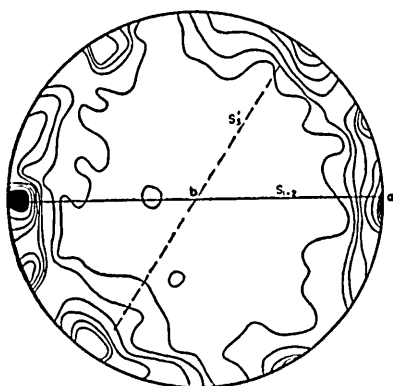


FIG. 35 a) 200 c-axes of quartz from sector A.

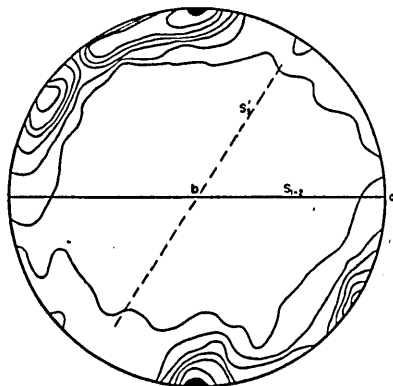


FIG. 35 b) 200 [001] of micas from sector A.

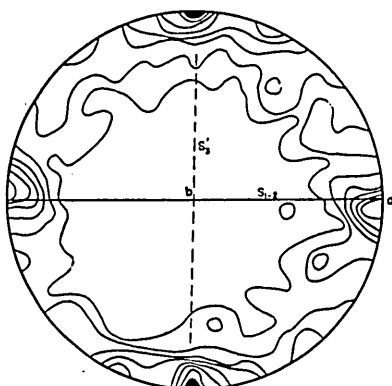


FIG. 36 200 c-axes of quartz from sector B.

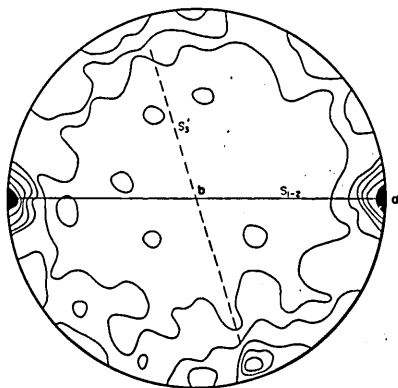


FIG. 37 a) 200 c-axes of quartz from sector C.

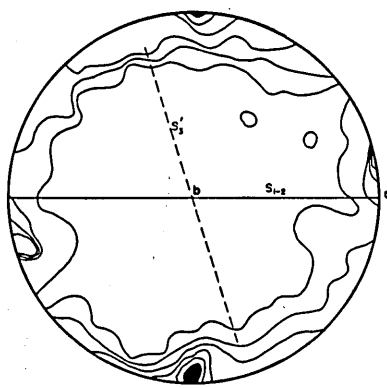


FIG. 37 b) 200 [001] of micas from sector C.

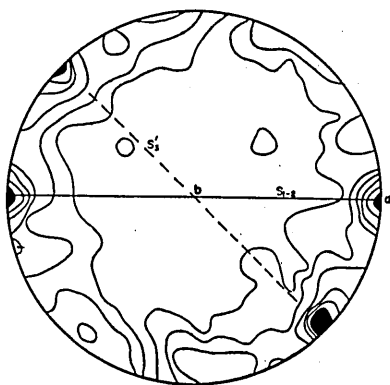


FIG. 38 200 c-axes of quartz from sector D.

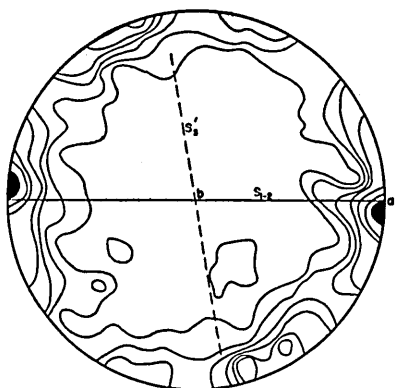


FIG. 39 a) 200 c-axes of quartz from sector E.

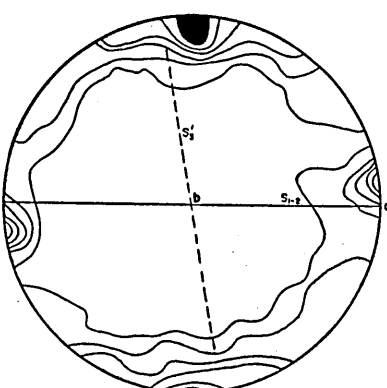


Fig. 39 b) 200 [001] of micas from sector E.

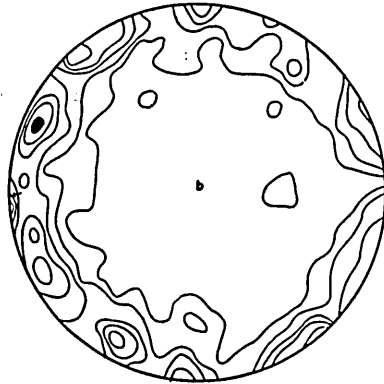


FIG. 40 200  $c$ -axes of quartz from sector F.

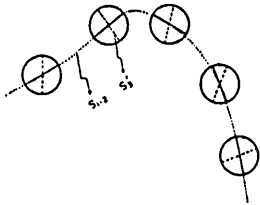


FIG. 41 Fan-formed orientation of  $S'_3$  in present fold form.

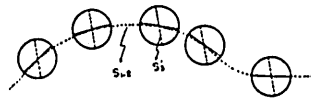


FIG. 42 Fold partially unfolded with  $S'_3$  parallel to one another.

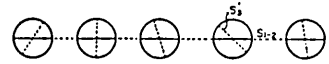


FIG. 43 Fold completely unfolded.

the influence of micro-folds of  $S_{1-2}$  described in preceding page.

Fig. 34 is the collective diagram of quartz made for the fold in its present form. The diagram is characterized by a remarkable spreading of  $c$ -axes of quartz on  $ac$  girdle, showing no available orientation pattern with reference to the axial surface of the fold. The fabric pattern is quite different from that in sectors A, B, C, D and E described above.

Though the presence of one set of  $(h0l)$ -surface and quartz submaximum corresponding to this surface in all the diagrams described above come into question, we can point out a possibility that the fold in question had been formed by flexure-slipping on  $S_{1-2}$ , on the basis of evidence described above. For reference purposes the  $(h0l)$ -surface is collectively designated as  $S'_3$ . Angular distance between  $S_{1-2}$  and  $S'_3$  is not constant through all sectors, and is between  $43^\circ$  and  $88^\circ$ . The  $S'_3$ -surfaces are approximately fan-shaped in distribution through the fold (Fig. 41). The fold in question is the type of "Fächerfalten" (SANDER, 1930, 1950) with reference to  $S'_3$ . The attitude of  $S'_3$  with reference to the fold is not dissimilar to that of the  $q$ -Richtungen of the quartz fold studied by LADURNER (1954). When the fold in question is partially unfolded until  $S'_3$  in each sector is aligned parallel to one another, a shallow troughed fold form is obtained (Fig. 42). This fold form may correspond to that of the phase, when the deformation related to the formation of  $S'_3$ , took place. Thus,

it may be concluded that the fold in question attained its present form through three stages of deformation as follows: 1) shear movement on  $S_{1-2}$  with the  $b$ -kinematic axis parallel to  $L_{2-3}$  ..... the formation of a shallow troughed fold form, 2) shear movement on the transversal surface  $S'_3$  with the  $b$ -kinematic axis parallel to  $L_{2-3}$  (Fig. 42), and 3) flexure-slipping on  $S_{1-2}$  with the  $b$ -kinematic axis parallel to  $L_{2-3}$ ... the formation of the present fold form.

## 2. Discussion

On the basis of careful examination about rock structures made in preceding pages, tectonic sequence in the older Ryoke deformation may be determined in order of younging as follows: 1)  $B_3$ -substage ... a) earlier  $B_3$ -substage, shear movement on  $S_{1-2}$  with the  $b$ -kinematic axis parallel to  $L_{2-3}$ , and b) later  $B_3$ -substage, deformation related to the formation of the transversal surfaces  $S_3$  and  $S_4$  with the  $b$ -kinematic axis parallel to  $L_{2-3}$  ... and 2)  $B_5$ -substage ... shear movement on  $S_{1-2}$  with the  $b$ -kinematic axis parallel to  $L_5$ . However, this does not mean that all the metamorphic rocks in the district had experienced the deformation of those styles progressively. It seems to be very important why during the progress of deformation its style in certain rocks was changed in such fashion as mentioned just above.

Though development of the  $B_5$ -fold and  $L_5$  is insignificant, they have been recognized through subareas C to K. Generally, the trend of them is only slightly oblique to that of  $L_{2-3}$ . As mentioned in preceding pages, it seems probable that the shear movement on  $S_{1-2}$  related to the formation of the  $B_5$ -folds and  $L_5$  did not take place sporadically within the district, but that the shear movement took place with the  $b$ -kinematic axis parallel to  $L_{2-3}$  in other many places within the district where the  $B_5$ -folds and  $L_6$  have not been recognized. The shear movement on  $S_{1-2}$  during the  $B_5$ -substage in question took place after the formation of the transversal surfaces  $S_3$  and  $S_4$ . The transversal surfaces  $S'_3$  in the  $B_5$ -fold examined in preceding pages may correspond to either one of  $S_3$  and  $S_4$  in non-folded rocks. If this inference is true, flexure-slipping on  $S_{1-2}$  with the  $b$ -kinematic axis parallel to  $L_{2-3}$  in the third stage of development of the  $B_3$ -fold will be synchronized with the shear movement on  $S_{1-2}$  during the  $B_5$ -substage. Thus, when above inference with respect to  $S'_3$  in the  $B_3$ -fold examined is true, it may be pointed out that the shear movement on  $S_{1-2}$  during the  $B_5$ -substage had taken place with the  $b$ -kinematic axis parallel to  $L_{2-3}$  in many places within the district.

The Sakawa granodioritic rocks had been intruded before the younger Ryoke deformation took place. In subarea K, remarkable variation in plunge of  $L_{2-3}$ -lineations has been recognized, and in some places they showed plunge of ca.  $55^\circ$ . However, the trend of lineation in the Sakawa granodioritic rocks in subarea K is constant, that gently plunging toward NNW. Therefore, the deformation related to the variation in plunge of  $L_{2-3}$  had taken place before or at least when the Sakawa granodioritic rocks were intruded into present geological and geographical level.

The  $S_5$ -surfaces, which appear to have been produced in close connection with the

B<sub>5</sub>-folding, have been recognized in some places of the peripheral zones of the Sakawa granodioritic rocks. Plate 20-2 indicates partial granitization of a zone of the S<sub>5</sub>-surfaces. In some examples, remarkable preferred orientation of sillimanite grains parallel to L<sub>5</sub>' on S<sub>5</sub> has been recognized (Plate 20-3 and 4). The fact, that the plastic flow on S<sub>1-2</sub> in the B<sub>5</sub>-substage became again active instead of the deformation related to the transversal surfaces S<sub>3</sub> and S<sub>4</sub>, seems to suggest rapid increase of plasticity of the rocks concerned, that may be ascribed to increase of temperature in the metamorphic field depending upon the approaching and intrusion of the Sakawa granodioritic rocks. The B<sub>3</sub>-folds and the B<sub>5</sub>-folds showing isoclinal-disharmonic style have been commonly recognized in the peripheral zones of the Sakawa granodioritic rocks. On the basis of those evidences and inferences, it may be safely concluded that the deformation in the B<sub>5</sub>-substage took place with close connection with the approach and intrusion of the Sakawa granodioritic rocks into present geological and geographical level and also subsequently to this intrusion, and that the B<sub>3</sub>-folds and the B<sub>5</sub>-folds showing isoclinal-disharmonic style may be correlated with highly plastic condition of the metamorphic rocks concerned depending upon the approach and intrusion of the Sakawa granodioritic rocks.

### C. MICA AND QUARTZ FABRICS

#### 1. Description

##### Specimen a

Locality: about 500 m to the north of Hirooka (subarea E)

Mineral composition: quartz, biotite, muscovite, and tourmaline

Original rock: chert

Principal schistosity S<sub>1-2</sub>: rather strong

Lination: L<sub>2-3</sub> moderately develops on S<sub>1-2</sub>.

Orientation pattern of [001] of micas is illustrated in Fig. 45. The diagram is characterized by an incomplete *ac* girdle with a maximum and two submaxima. The maximum corresponds strictly to S<sub>1-2</sub>, and the two submaxima represent the presence of two sets of (*hOl*)-surfaces, which are almost symmetrically oriented to S<sub>1-2</sub>. The quartz diagram (Fig. 44) is characterized by a maximum and two submaxima on the *ac* great circle. The maximum shows the position of Maximum I after SANDER with reference to S<sub>1-2</sub>. Also the two submaxima are Maximum I with reference to two sets of (*hOl*)-surfaces, respectively. Thus, it may be concluded that those fabrics were produced by the deformation with the *b*-kinematic axis parallel to L<sub>2-3</sub>, accordingly by the older Ryoke deformation.

##### Specimen b

Locality: Hirooka (subarea E)

Mineral composition: quartz, plagioclase, biotite, muscovite, cordierite and tourmaline

Original rock: psamitic rock

Principal schistosity S<sub>1-2</sub>: rather imperfect

Lination: L<sub>2-3</sub> moderately develops on S<sub>1-2</sub>.

The mica diagram (Fig. 47) is characterized by a complete *ac* girdle with a maximum and two submaxima. The maximum corresponds strictly to  $S_{1-2}$ , and the two submaxima represent the presence of two sets of (*hOl*)-surfaces, which are almost symmetrically oriented to  $S_{1-2}$ . The quartz diagram (Fig. 46) is characterized by a complete *ac* girdle with a maximum and two submaxima. The two submaxima are Maximum I with reference to the two sets of (*hOl*)-surfaces. However, the maximum, which are present away from the *ac* great circle, seems to be difficult to interpret in term of  $S_{1-2}$  or the (*hOl*)-surface. However, it may be concluded that main feature of the quartz fabric (*ac* girdle and two submaxima) was produced by the deformation with the *b*-kinematic axis parallel to  $L_{2-3}$ .

Specimen c

Locality: Hirooka (western end of subarea F)

Mineral composition: quartz, plagioclase, biotite and garnet

Original rock: chert

Principal schistosity  $S_{1-2}$ : rather imperfect

Lination:  $L_{2-3}$  develops moderately.

The mica diagram (Fig. 49) is characterized by a complete *ac* girdle with a maximum and two submaxima. The maximum corresponds strictly to  $S_{1-2}$ , and the two submaxima represent the presence of two sets of (*hOl*)-surfaces, which are almost symmetrically oriented to  $S_{1-2}$ . The quartz diagram (Fig. 48) is characterized by a sharply defined *ac* girdle with a maximum and four submaxima. The maximum is Maximum I with reference to the one of two sets of (*hOl*)-surfaces. The submaxima seem not to be related to any one of  $S_{1-2}$  and the (*hOl*)-surface with respect to their positions, though they exist on the *ac* great circle. The symmetry of the mica and quartz fabrics described above is approximately monoclinic with a single symmetry plane normal to  $L_{2-3}$  in common. Thus, it may be concluded that main feature of those fabrics was produced by the deformation with the *b*-kinematic axis parallel to  $L_{2-3}$ .

Specimen d

Locality: about 500 m to the east of Hirooka (subarea F)

Mineral composition: quartz, plagioclase, biotite, muscovite and garnet

Original rock: chert

Principal schistosity  $S_{1-2}$ : rather imperfect

Lination:  $L_{2-3}$  develops moderately.

The mica diagram (Fig. 51) is characterized by an incomplete *ac* girdle with a maximum and two submaxima. The maximum corresponds strictly to  $S_{1-2}$ , and the two submaxima represent the presence of two sets of (*hOl*)-surfaces, which are almost symmetrically oriented to  $S_{1-2}$ . The symmetry of the mica fabric is monoclinic with a single symmetry plane normal to  $L_{2-3}$ , that suggesting that it was produced by the deformation with the *b*-kinematic axis parallel to  $L_{2-3}$ .

The quartz diagram (Fig. 50) shows weak concentration and less regular pattern. The pattern is decidedly triclinic. The maximum (only 3 per cent) in the diagram

is Maximum I with reference to  $S_{1-2}$ . However, many of  $c$ -axes of quartz in the diagram tend to be present away from the  $ac$  great circle, unlike the quartz fabrics of specimens, a, b, and c.

Specimen e

- Locality: Kasagi
- Mineral composition: quartz, plagioclase, biotite, muscovite and garnet
- Original rock: chert
- Principal schistosity  $S_{1-2}$ : rather imperfect
- Lineation:  $L_{2-3}$  develops weakly.

The mica diagram is characterized by an incomplete  $ac$  great circle girdle with a maximum and a submaxima (Fig. 53). The maximum corresponds strictly to  $S_{1-2}$ , and the submaximum represents the presence of one set of  $(h0l)$ -surface. When compared with the mica fabrics of specimens a, b, c and d, in this mica fabric amount of  $[001]$ -axes of micas, which are present away from the  $ac$  great circle, increases relatively. However, the mica fabric shows rather monoclinic symmetry than triclinic.

While, the quartz fabric shows decidedly triclinic symmetry (Fig. 52). Many of  $c$ -axes of quartz in the diagram tend to be present away from the  $ac$  great circle. The pattern is characterized by an incomplete small circle girdle with six maxima (3 per cent) with an angular radius of ca.  $63^\circ$ , the center of which coincides with the fabric axis  $b$ . The six maxima can be grouped as three maximum groups. Those maximum groups are Maximum IV after SANDER with reference to  $S_{1-2}$ .

Specimen f

- Locality: near center of subarea I
- Mineral composition: quartz, plagioclase, biotite, muscovite, garnet and tourmaline
- Original rock: chert
- Principal schistosity  $S_{1-2}$ : rather strong, approximately flat-lying
- Lineation:  $L_{2-3}$  develops rather weakly.

The mica fabric diagram shows rather triclinic symmetry (Fig. 55). However, the fabric pattern is characterized by a sharply defined  $ac$  great circle girdle with a maximum and two submaxima. The maximum corresponds strictly to  $S_{1-2}$ , and two submaxima represent the presence of two sets of  $(h0l)$ -surfaces, which are almost symmetrically oriented to  $S_{1-2}$ . It is no doubt that these components in the mica fabric had been produced by the deformation with the  $b$ -kinematic axis parallel to  $L_{2-3}$ , as well as the mica fabrics of specimens described above.

Also the quartz diagram shows triclinic symmetry (Fig. 54). Concentration of  $c$ -axes of quartz on the  $ac$  great circle is very low. The fabric pattern is not dissimilar to that of Diagram (1) of H. W. FAIRBAIRN (1954). That is, main feature of the quartz fabric in question is a sharply defined small circle girdle with an angular radius of ca.  $60^\circ$ , the center of which coincides with the fabric axis  $b$ .

Specimen g

- Locality: about 500 m to the northwest of Kodono (subarea J)

Mineral composition: quartz, plagioclase, biotite, muscovite, garnet and tourmaline

Original rock: chert

Principal schistosity  $S_{1-2}$ : rather imperfect

Lamination:  $L_{2-3}$  develops weakly.

The mica diagram shows rather triclinic symmetry (Fig. 57). However, this is characterized by a sharply defined  $ac$  great circle girdle with a maximum and a submaximum. The maximum corresponds strictly to  $S_{1-2}$ , and the submaximum represent one set of  $(h0l)$ -surface. Concentration of  $[001]$ -axes of micas in zone away from the  $ac$  great circle tends to increase, when compared with the mica fabrics of specimens a to e.

The quartz diagram (Fig. 56) shows weak concentration and less regular pattern. The pattern is triclinic. The maximum (3 per cent) is Maximum I with reference to  $S_{1-2}$ . The trends of girdles containing the maximum and submaxima in the diagram show very peculiar pattern. They can be classified into two types as follows: 1) a sharply defined  $ac$  great circle girdle, and 2) girdles approximately perpendicular to the fabric plane  $ac$ .

Specimen h

Locality: about 1000 m to the south of Nishioku (southern end of subarea I)

Mineral composition: quartz, plagioclase, biotite, muscovite, and garnet

Original rock: chert

Principal schistosity  $S_{1-2}$ : rather distinct

Lamination:  $L_{2-3}$  is only faintly recognizable.

The mica diagram shows triclinic symmetry (Fig. 59). However, main feature of fabric pattern is a sharply defined incomplete  $ac$  great circle girdle with a maximum (corresponding to  $S_{1-2}$ ) and two submaxima (representing the presence of two sets of  $(h0l)$ -surfaces). Also in zone away from the  $ac$  great circle is observed higher concentration of  $[001]$ -axes of micas, like in the mica fabrics of specimens f and g described above.

The quartz fabric shows triclinic symmetry (Fig. 58). The  $c$ -axes of quartz tend to orient on a small circle with an angular radius of ca.  $60^\circ$ , the center of which coincides with the fabric axis  $b$ . However, main feature of the quartz fabric is one maximum group and one submaximum on the small circle.

Specimen i

Locality: about 500 m to the west of Kodono (subarea J)

Mineral composition: quartz, plagioclase, biotite, muscovite and garnet

Original rock: chert

Principal schistosity  $S_{1-2}$ : rather imperfect

Lamination:  $L_{2-3}$  is faintly recognized, and  $L_6$  develops distinctly.

The mica fabric (Fig. 61) shows triclinic symmetry. This mica fabric represents two components of fabric pattern: 1) an incomplete  $ac$  great circle girdle with a maximum and two submaxima, and 2) an incomplete small circle girdle with two submaxima with an angular radius of ca.  $56^\circ$ , the center of which coincides with the

fabric axis  $b$ . The maximum corresponds strictly to  $S_{1-2}$ , and the two submaxima on the  $ac$  great circle represent the presence of two sets of  $(hOl)$ -surfaces, which are almost symmetrically oriented to  $S_{1-2}$ . It is no doubt that this first component of fabric pattern was produced by the deformation with the  $b$ -kinematic axis parallel to  $L_{2-3}$ . The two submaxima on the small circle (the second component) represent the presence of two sets of surfaces which are symmetrically oriented with inclination of ca.  $34^\circ$  to  $S_{1-2}$ . The line of intersection of these two sets of surfaces and  $S_{1-2}$  coincides strictly with  $L_6$  normal to  $L_{2-3}$ . Therefore, they are  $(OkI)$ -surfaces.  $L_6$  must be the trace of the  $(OkI)$ -surfaces on  $S_{1-2}$ . From the macroscopic geometry of  $S_{1-2}$ ,  $L_6$  and  $B_6$ -fold, it was pointed out that the axis of  $B_6$ -fold and  $L_6$  correspond to the  $b$ -kinematic axis (within each of small fields of the district) in the younger Ryoke deformation. Therefore, it may be concluded that those two sets of  $(OkI)$ -surfaces correspond to a pair of shear surfaces formed by the deformation of the type of two dimensional flattening acted from the direction parallel or perpendicular to  $S_{1-2}$ , and that  $L_6$  coincides with the single symmetry axis of this deformation. Those two sets of  $(OkI)$ -surfaces are designated as  $S_6$  and  $S_7$ , respectively.

The quartz fabric shows a very peculiar pattern with rather triclinic symmetry (Fig. 60). The fabric pattern is characterized by a small circle girdle with two maxima with an angular radius of ca.  $34^\circ$ , the center of which coincides with the fabric axis  $b$ . The pattern is geometrically harmonic with that of micas described in term of the second component in the mica fabric. The two quartz maxima show the position of Maximum I with reference to the two sets of  $(OkI)$ -surfaces. Thus, it may be concluded that the quartz orientation was developed by the deformation (the younger Ryoke deformation) which formed the second component of fabric pattern in the mica fabric.

Specimen j

Locality: Obane (southern end of subarea J)

Mineral composition: quartz, plagioclase, biotite and garnet.

Original rock: chert

Principal schistosity  $S_{1-2}$ : distinct

Lination:  $L_6$  develops distinctly.  $L_{2-3}$  is faintly recognized.

The fabric diagrams (Figs. 63 and 62) for mica and quartz have been established from thin section perpendicular to the axis of the  $B_6$ -fold trending approximately normal to  $L_{2-3}$ .

The mica fabric is characterized by two sharply defined great circle girdles and a maximum. The one is the incomplete  $ac$  great circle girdle, and the other is the complete  $bc$  great circle girdle. The maximum corresponds strictly to  $S_{1-2}$ . The development of two separate great circle girdles in the mica fabric seems to suggest that the rocks concerned experienced two distinct deformation. It is obvious that the  $ac$  great circle girdle is correlated with the deformation with the  $b$ -kinematic axis parallel to  $L_{2-3}$ , and that the  $bc$  great circle girdle is correlated with the deformation related to the formation of the  $B_6$ -folds and  $L_6$ .

On the other hand, the quartz fabric shows a simple pattern with monoclinic symmetry. The pattern is characterized by a sharply defined  $bc$  great circle girdle with a maximum and a submaximum. The maximum shows the position of Maximum I with reference to  $S_{1-2}$ . Thus, it may be safely concluded that the quartz orientation had been developed by the deformation related to the  $B_6$ -folds and  $L_6$ .

Specimen k

Locality: about 1000 m to the northeast of Sakawahigashi (subarea K)

Mineral composition: quartz, plagioclase, biotite, muscovite, sillimanite, and garnet

Original rock: sandstone

Schistosity surface: Only the  $S_5$ -surfaces develops distinctly.

Lination:  $L'_5$  develops distinctly.

The mica fabric is illustrated in Fig. 65. The fabric pattern is characterized by an incomplete great circle girdle with a maximum and two submaxima, showing monoclinic symmetry. The maximum corresponds strictly to  $S_5$ , and the two submaxima represent the presence of two sets of  $(h0l)$ -surfaces with reference to  $L'_5$ , which are almost symmetrically oriented to  $S_5$ . It is no doubt that the mica fabric was produced by the deformation with the  $b$ -kinematic axis parallel to  $L'_5$ .

While, the quartz fabric shows triclinic symmetry (Fig. 64). The pattern is characterized by an incomplete small circle girdle with five maxima (3 per cent) with an angular radius of ca.  $68^\circ$ , the center of which coincides with the fabric axis  $b$  ( $L'_5$ ). The two maxima have no separate significance and can be grouped together as one maximum group. The three maxima and one maximum group are Maximum IV after SANDER with reference to  $S_5$ .

Specimen l

Locality: Kiriya (subarea D)

Mineral composition: quartz, plagioclase, biotite, muscovite, and tourmaline

Original rock: sandstone

Principal schistosity  $S_{1-2}$ : distinct

Lination:  $L_{2-3}$  develops distinctly. Also  $L_5$  is visibly recognized.

The mica fabric is illustrated in Fig. 67. The pattern is characterized by a sharply defined  $ac$  great circle girdle with a maximum, showing nearly orthorhombic symmetry. The maximum corresponds strictly to  $S_{1-2}$ .

While, the quartz fabric (Fig. 66) shows triclinic symmetry. Main feature of fabric pattern is a sharply defined incomplete small circle girdle with two maxima and two submaxima with an angular radius of ca.  $65^\circ$ , the center of which coincides with the fabric axis  $b$ . The maxima and submaxima are approximately Maximum IV with reference to  $S_{1-2}$ . The pattern of quartz fabric just described is similar to that of specimens e and h. The effect of the deformation related to  $L_5$  cannot be seen in the mica and quartz fabrics.

Specimen m

Locality: about 500 m to the east of Kiriya (Subarea D)

Mineral composition: quartz, biotite and muscovite

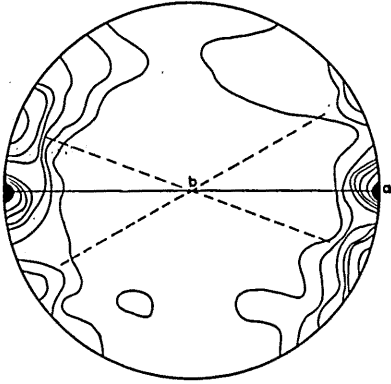


FIG. 44 400 c-axes of quartz in specimen a;  
Contours 6-5-4-3-2-1%.

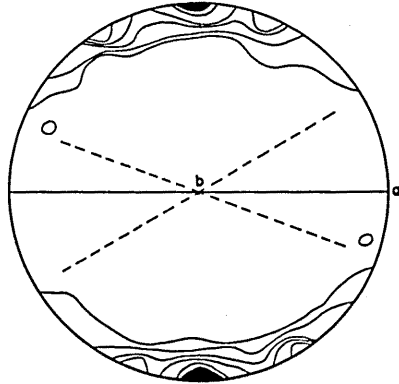


FIG. 45 200 [001] of micas in specimen a;  
Contours 11-9-7-5-3-1%.

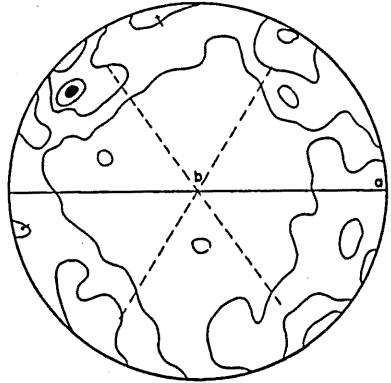


FIG. 46 400 c-axes of quartz in specimen b;  
Contours 4-3-2-1%.

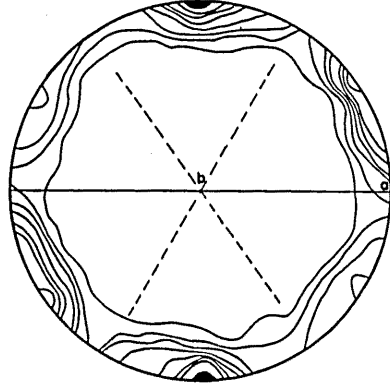


FIG. 47 200 [001] of micas in specimen b;  
Contours 10-8-6-5-4-3-2-1%.

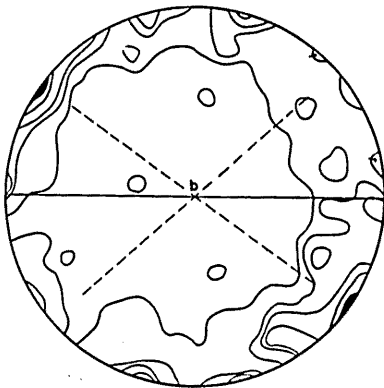


FIG. 48 400 c-axes of quartz in specimen c;  
Contours 5-4-3-2-1%.

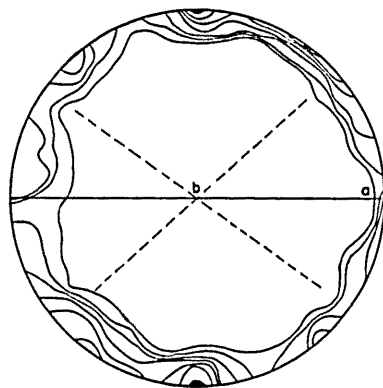


FIG. 49 200 [001] of micas in specimen c;  
Contours 11-9-7-5-3-2-1%.

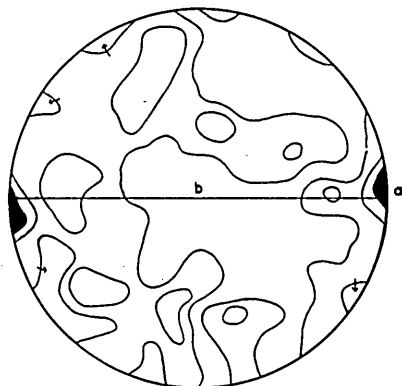


FIG. 50 400 c-axes of quartz in specimen d;  
Contours 3-2-1%.

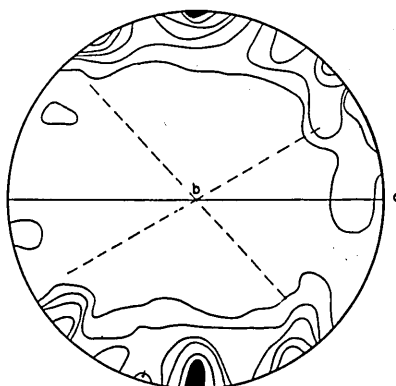


FIG. 51 200 [001] of micas in specimen d;  
Contours 9-7-5-3-2-1%.

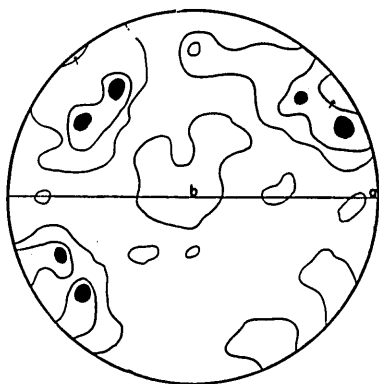


FIG. 52 400 c-axes of quartz in specimen e;  
Contours 3-2-1%.

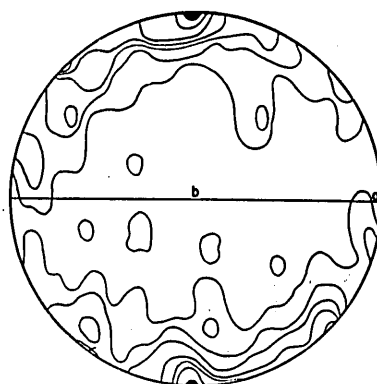


FIG. 53 200 [001] of micas in specimen e;  
Contours 9-7-5-4-3-2-1%.

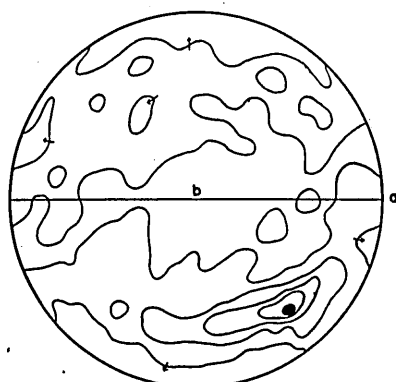


FIG. 54 400 c-axes of quartz in specimen f;  
Contours 5-4-3-2-1%.

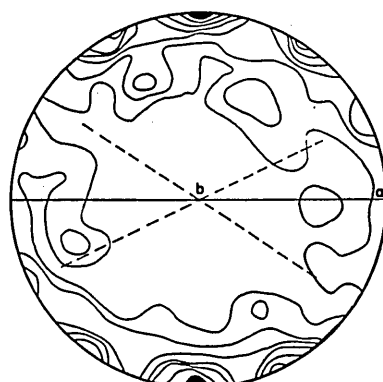


FIG. 55 200 [001] of micas in specimen f;  
Contours 10-8-6-4-3-2-1%.

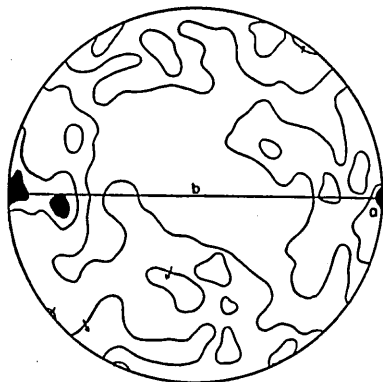


FIG. 56 400 c-axes of quartz in specimen g;  
Contours 3-2-1%.

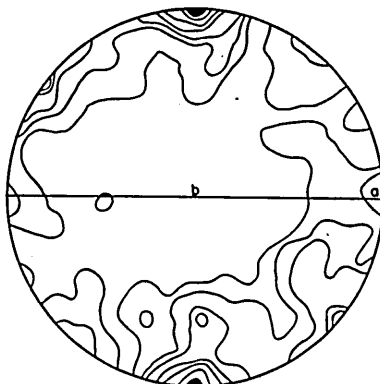


FIG. 57 200 [001] of micas in specimen g;  
Contours 10-8-6-4-3-2-1%.

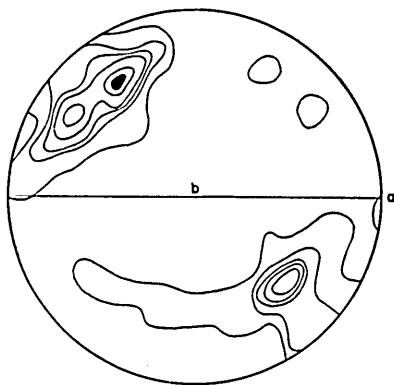


FIG. 58 400 c-axes of quartz in specimen h;  
Contours 6-5-4-3-2-1%.

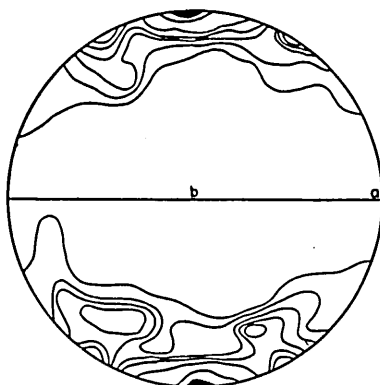


FIG. 59 200 [001] of micas in specimen h;  
Contours 15-10-5-4-3-2-1%.

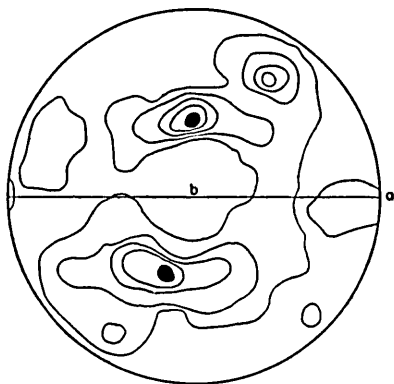


FIG. 60 400 c-axes of quartz in specimen i;  
Contours 5-4-3-2-1%.

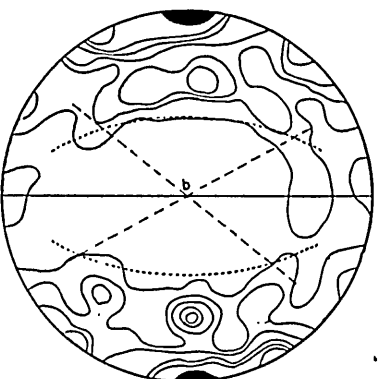


FIG. 61 200 [001] of micas in specimen i;  
Contours 7-5-4-3-2-1%.

Studies on the Structure of the Ryoke Metamorphic Rocks of the Kasagi District, Southwest Japan

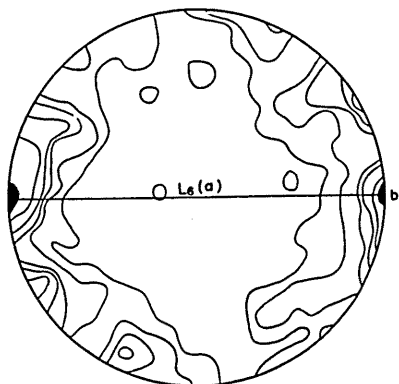


FIG. 62 400 *c*-axes of quartz in specimen *j*;  
Contours 6-5-4-3-2-1%.

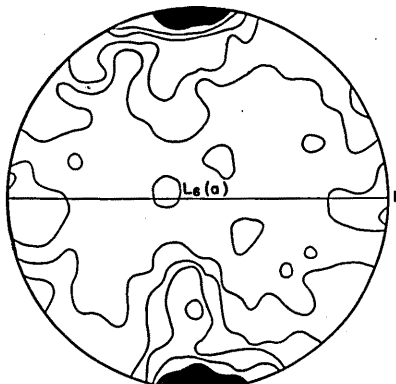


FIG. 63 200 [001] of biotite flakes in specimen  
*j*; Contours 9-7-5-3-1%.

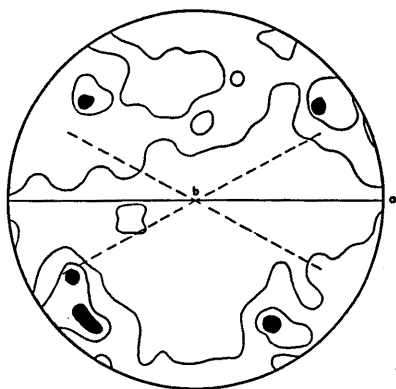


FIG. 64 500 *c*-axes of quartz in specimen *k*;  
Contours 3-2-1%.

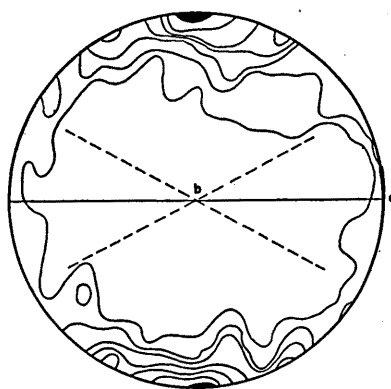


FIG. 65 200 [001] of micas in specimen *k*;  
Contours 10-8-6-4-3-2-1%.

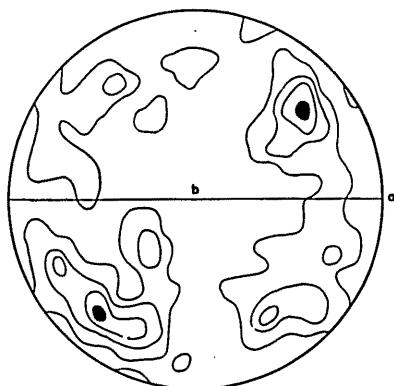


FIG. 66 500 *c*-axes of quartz in specimen *l*;  
Contours 4-3-2-1%.

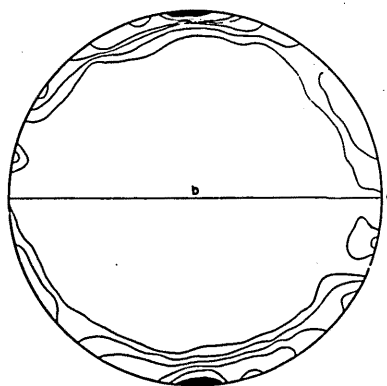


FIG. 67 200 [001] of micas in specimen *l*;  
Contours 13-10-7-5-3-1%.

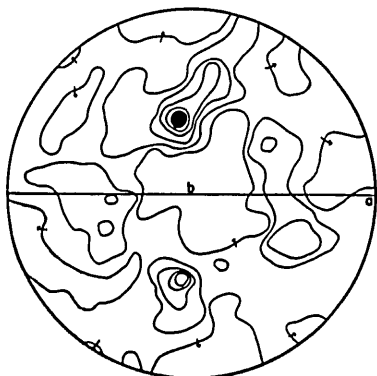


FIG. 68 400 *c*-axes of quartz in specimen *m*;  
Contours 6-5-4-3-2-1%.

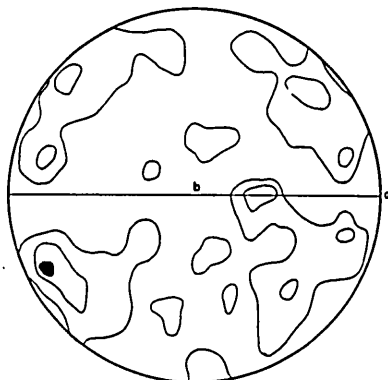


FIG. 69 500 *c*-axes of quartz in specimen *n*;  
Contours 3-2-1%

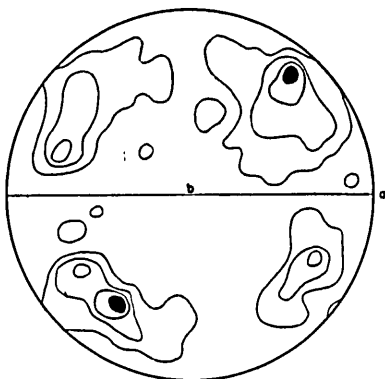


FIG. 70 500 *c*-axes of quartz in specimen *o*; Contours 4-3-2-1%.

Original rock: chert:

Principal schistosity: rather imperfect

Lination:  $L_{2-3}$  develops distinctly.

The quartz fabric (Fig. 68) is characterized by a complete small circle girdle with a maximum and a submaximum with an angular radius of ca.  $35^\circ$ , the center of which coincides with the fabric axis *b*. The maximum and submaximum lie on the fabric plane *bc* and are symmetrically oriented with inclination of  $35^\circ$  to  $S_{1-2}$ . The pattern of quartz fabric just described is similar to that of specimen *i*. However, the patter of mica fabric of this specimen is quite similar to that of specimen *l*.

The quartz fabric (Figs. 69 and 70) established from other specimens (*n* and *o*) in subareas B and C show similar fabric pattern to that of the quartz fabric of specimen *l*.

## 2. Summary and discussions

- (1) The mica fabrics described in preceding pages are classified into following

three types. 1) The first type is the mica fabrics of specimens a, b, c, d, e, f, g, h and l. They show the  $ac$  great circle girdle with the maximum, which corresponds strictly to  $S_{1-2}$ , and in many of them two submaxima on the  $ac$  great circle, which represent the presence of two sets of  $(h0l)$ -surfaces almost symmetrically oriented to  $S_{1-2}$ . Judging from the close association of those two sets of  $(h0l)$ -surfaces and their symmetrical disposition with respect to  $S_{1-2}$  in many of the specimens examined, they seem to correspond to a pair of shear surfaces formed by the deformation of the type of two dimensional flattening, just as the conjugate transversal surfaces  $S_3$  and  $S_4$  in metamorphic derivatives from pelitic and semi-pelitic rocks in subareas B, C, and D. Those two sets of  $(h0l)$ -surfaces in question may be correlated with the  $S_3$ - and  $S_4$ -surfaces. Passing from specimen a to specimen h, the concentration of  $[001]$ -axes of micas tends to increase progressively in the zone away from the  $ac$  great circle. 2) The second type is the mica fabric of specimen i, which is characterized by the distinct  $L_6$ -lineation. It represents two components of fabric pattern: a) an incomplete  $ac$  great circle girdle with a maximum and two submaxima (corresponding to  $S_3$  and  $S_4$ ), and b) an incomplete small circle girdle with two submaxima with an angular radius of ca.  $56^\circ$ , the center of which coincides with the fabric axis  $b$ . These submaxima represent the presence of two sets of  $(0kl)$ -surfaces, which are almost symmetrically oriented to  $S_{1-2}$ . 3) The third type is the mica fabric of specimen j collected from the limb of  $B_6$ -fold. It is characterized by two sharply defined great circle girdles parallel to the  $ac$  and  $bc$  great circle respectively.

(2) The quartz diagrams described in preceding pages are classified into following four types. 1) The first type is the quartz fabrics of specimens a, and b collected from subarea E together. They are characterized by the  $ac$  great circle girdle with maximum and submaxima. The maximum and submaxima generally correspond to the position of Maximum I after SANDER with reference to  $S_{1-2}$ ,  $S_3$  and  $S_4$ , respectively. The first type of quartz fabric is correlated with that of mica fabric. However, the first type of mica fabric can not be always correlated with that of quartz fabric. 2) The second type is the quartz fabric of specimen i, which is characterized by the distinct  $L_6$ -lineation. That is characterized by two maxima and a small circle girdle with an angular radius of ca.  $34^\circ$ , the center of which coincides with the fabric axis  $b$ . The two maxima represent the position of Maximum I with reference to the  $(0kl)$ -surfaces ( $S_6$  and  $S_7$ ). The second type of quartz fabric is correlated with that of mica fabric. 3) The third type is the quartz fabric of specimen j collected from the limb of  $B_6$ -fold. It is characterized by a sharply defined  $bc$  great circle girdle with a maximum and a submaximum. The maximum represent the position of Maximum I with reference to  $S_{1-2}$ . The third type of quartz fabric is correlated with that of mica fabric. 4) The fourth type is the quartz fabric of specimens e, f, h, k, l, n and o. In the diagram many of  $c$ -axes of quartz tend to be present away from the  $ac$  great circle. The pattern is characterized by an incomplete small circle girdle with maxima, the center of which coincides with the fabric axis  $b$ . The angular radius of small circle girdle is between  $60^\circ$  and  $70^\circ$ . The fourth type of

quartz fabric is correlated with the first type of mica fabric.

(3) Now we will ask as follows: Is it due to what cause that the first type of mica fabric is correlated with both the first and the fourth type of quartz fabric? and whether is the fourth type of quartz fabric correlated with deformative movement with a deformation plane perpendicular to the fabric axis  $b$ , just as well as the first type of quartz and mica fabric?

(4) In the quartz diagrams of specimens  $c$ ,  $d$  and  $g$ , the  $c$ -axes of quartz tend to concentrate in a broad zone making angles of between  $60^\circ$  and  $90^\circ$  with the direction of the fabric axis  $b$ . It may be pointed out that they correspond to the intermediate type between the first and the fourth type. Passing from the first type of quartz fabric, through the intermediate type, to the fourth type, the corresponding change in the mica fabrics is analogous increase of number of the  $[001]$ -axes of micas which are present away from the  $ac$  great circle.

(5) Fig. 71 shows the trends of girdles containing the maxima and submaxima in the quartz diagrams of specimens  $b$ ,  $c$ ,  $d$ ,  $e$ ,  $f$ ,  $g$ ,  $h$ ,  $k$ ,  $l$ ,  $n$  and  $o$  (belonging to the first, the fourth and the intermediate type of quartz fabric). Most of the girdles are present within a broad zone making angles of between  $50^\circ$  and  $90^\circ$  with the direction of the fabric axis  $b$ . The girdles can be classified into following two types: 1) the incomplete  $ac$  small circle girdle, and 2) the incomplete girdle perpendicular to the fabric plane  $ac$ . Analogous diagram for the trends of girdles containing the maxima was reported by FAIRBAIRN (1949). The close association of the first type and the second type of girdle pattern seems to be very important.

(6) The present author (1961) pointed out that the  $c$ -axes of quartz must be stably oriented at ca.  $30^\circ$  to the direction of the maximum compression axis. Therefore, when an appropriate rock was uniformly compressed from all the directions within the fabric plane  $ac$  accompanied with axial extension parallel to the fabric axis  $b$ , the newly induced quartz fabric may represent a small circle girdle with maxima and submaxima with an angular radius of ca.  $60^\circ$ , the center of which coincides with the fabric axis  $b$  (Fig. 72-B). Also, when an appropriate rock was axially compressed from the direction of the fabric axis  $b$  accompanied with equal amount of extension in all of the directions within the fabric plane  $ac$ , the newly induced quartz fabric may represent a small circle girdle with maxima and submaxima with an angular radius of ca.  $30^\circ$ , the center of which coincides with the fabric axis  $b$  (Fig. 72-A). Based on the experimental research, GRIGGS *et al.* (1960) said, "the  $c$ -axes of the calcite grains tend to remain in a plane in which lie the axis of tension and the direction of concentration of  $c$ -axes in the initial fabric. ....And even at strains exceeding 500 per cent the influence of the initial preferred orientation pattern upon evolution of the new fabric is still highly effective". This conclusion must be valid for orienting mechanism of quartz lattice in deformed rock.

(7) Thus, the quartz fabric of the fourth type, which is characterized by the incomplete small circle girdle with maxima and submaxima with angular radius of between  $60^\circ$  and  $70^\circ$ , the center of which coincides with the fabric axis  $b$ , may be

correlated with the compressive stress in equal amount in all the directions within the fabric plane  $ac$  accompanied with axial extension parallel to the fabric axis  $b$ . The girdles perpendicular to the fabric plane  $ac$  in Fig. 71 may represent progressive migration of quartz axes under the newly directed stress system assumed above from the  $ac$  great circle, in which most of the quartz axes were concentrated as in the first type of quartz fabric. Thus, it may be pointed out that the quartz fabric of the fourth type had evolved from that of the first type by the action of above assumed stress system. The association of the mica fabrics of the first type and the quartz fabrics of the fourth type, between which distinct symmetrological discrepancies are observed, seems to be illustrated in Kvale's following terms: "... the quartz grains reflect a later stage of deformation than do the micas." (KVALE, 1953). Passing from the first type of quartz fabric, through the intermediate type, to the fourth type, in the corresponding mica fabrics the concentration of [001]-axes of micas tends to increase progressively in the zone away from the  $ac$  great circle, that probably reflecting weakly the deformation related to the formation of quartz fabrics of the fourth type.

(8) Now the origin of the assumed stress system responsible for the formation of the quartz fabric of the fourth type comes into question. As discussed in preceding pages, both the first type of mica fabric and that of quartz fabric were correlated with the older Ryoke deformation. After the older Ryoke deformation with the  $b$ -kinematic axis having east-west regional trend ceased, the rocks which had experienced the older Ryoke deformation was refolded with respect to the axis of external rotation vertically plunging with reference to the geological coordinates as a whole, accompanied with the formation of the  $B_6$ -folds and  $L_6$ -lineations corresponding to the  $b$ -kinematic axis within each of small fields of the district (the younger Ryoke deformation). The "principal stress" originated in folded layers during the younger Ryoke deformation may correspond to the assumed stress system responsible for the quartz fabric of the fourth type. As mentioned in preceding pages, the second type of mica and quartz fabrics, which develop in the rock with the distinct  $L_6$ -lineation, and the third type of mica and quartz fabrics, which develop in the rock collected from the limb of  $B_6$ -fold, were correlated with the deformation related to the formation of  $L_6$ -lineation and  $B_6$ -fold respectively, that is, with the younger Ryoke deformation.

(9) A common characteristic feature between the quartz fabrics of the first, the second and the third type is that the maximum in the diagram represent the position of Maximum I after SANDER with reference to either one of the schistosity surfaces in the rocks concerned. In preceding pages, the maximum in question was correlated with the plastic flow on the corresponding schistosity surface in the rocks concerned, according to SANDER's hypothesis (1950). On the other hand, the quartz fabric of the fourth type were reasonably illustrated on the basis of the present author's hypothesis that the quartz grains are stably oriented with their  $c$ -axes at ca.  $30^\circ$  to the compression axis or at ca.  $60^\circ$  to the tension axis. Now, the relationship between

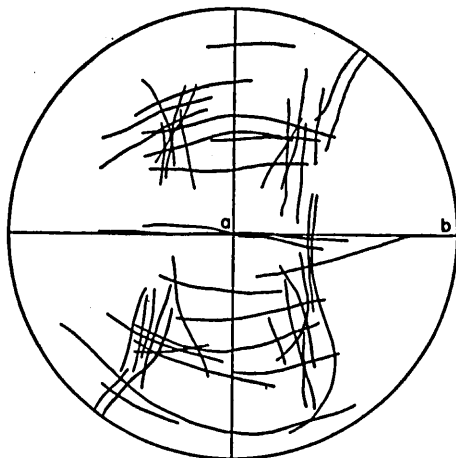


FIG. 71 Composite diagram showing the trends of the girdles containing the maxima and sub-maxima in quartz diagrams of specimens b, c, d, e, f, g, h, k, l, n and o.

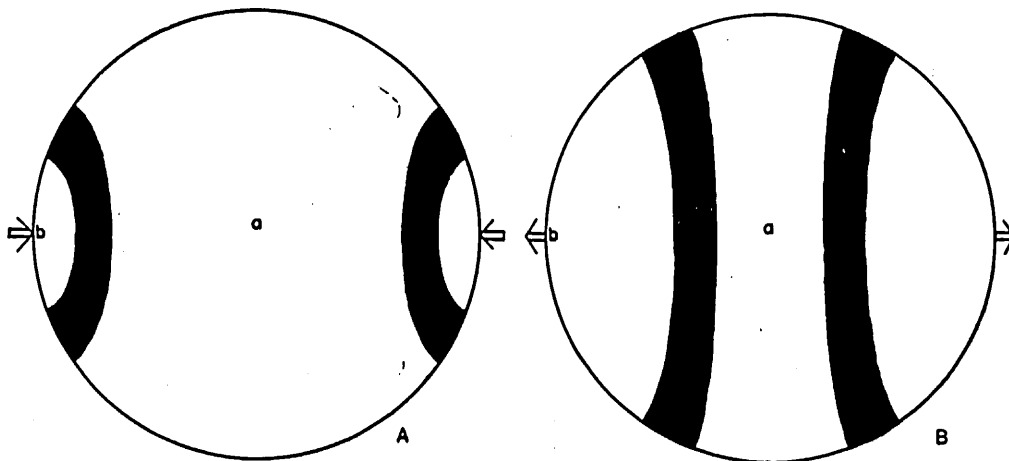


FIG. 72 Ideal orientation diagram for *c*-axes of quartz.

A) Stable orientation of *c*-axes (black bands) under compressive stress directed parallel to the fabric axis *b*, accompanied with equal amount of extension in all of the directions within the fabric plane *ac*.

B) Stable orientation of *c*-axes (black bands) under tensile stress directed parallel to the fabric axis *b*, accompanied with equal amount of compression in all of the directions within the fabric plane *ac*.

SANDER'S hypothesis and the present author's comes into question.

## VI CONCLUDING REMARKS

Some of the results made clear through the discussion in the preceding pages will be summarized in following, along with some geological and petrological meanings

TABLE 1

Deformation	Plutonism	Metamorphism
Tamba deformation		
Older Ryoke deformation { B <sub>3</sub> -substage { B <sub>2</sub> -substage	Sakawa granodioritic rocks	Older Ryoke metamorphism
Younger Ryoke deformation	Yagyu granite	Younger Ryoke metamorphism
	Koya granodioritic rocks	ditto (?)
Post Ryoke deformation		

deducible from them (Table 1).

The conclusion that main rock- and geologic structures in subarea A had been produced before the Ryoke metamorphism took place and that the similar type of structures can be traced all over other subareas, although those structures were almost completely reconstructed in these subareas by the deformations during the Ryoke metamorphic phase, have been pointed out on the basis of consideration about the geometrical relation between the B<sub>1</sub>-folds and S<sub>1-2</sub>-surfaces and between the B<sub>1</sub>-fold and the mica fabric. The main rock- and geologic structures observed in subarea A have been traced in quite similar fashion in the Tamba zone (in the southern half of Kyoto Pref.) north of the district, where they have been scarcely destroyed by later deformations. They correspond to the main rock- and geologic structures in the Tamba zone which show east-west regional trend as a whole. It is, therefore, pointed out that similar rock- and geologic structures, to what are observed in the Tamba zone (in the southern half of Kyoto Pref.) at present, developed all over the Kasagi district prior to the Ryoke metamorphism. The deformation related to the formation of those rock- and geologic structures is the Tamba deformation (*cf.* HARA, 1959, 1960).

The boundary line between the Tamba and the Ryoke zone can not strictly be drawn as a line. From the viewpoint of metamorphic recrystallization of the rocks concerned, the boundary line in question coincides with a line, along which non-metamorphic slates (in the Tamba zone) change to biotite-bearing slates (in the Ryoke zone). In the Kasagi district, however, the boundary line in this sense does not correspond to that with reference to the rock- and geologic structures. While the rocks in subarea A are recrystallized by the older Ryoke metamorphism and characterized by recrystallized biotite flakes, main features of the rock- and geologic structures in this subarea are quite similar to those of non-metamorphic rocks in the Tamba zone. The style of rock- and geologic structures changes suddenly within subarea B. The structure of the S<sub>1-2</sub>-surfaces in subareas C and D shows monoclinic symmetry with a single symmetry plane normal to L<sub>2-3</sub>-lineation related to the older Ryoke deformation during the Ryoke metamorphic phase. The boundary line

between the Tamba and the Ryoke zone with special reference to the rock- and geologic structures must be drawn through subarea B.

The older Ryoke deformation took place with respect to the *b*-kinematic axis with the east-west regional trend (parallel to the regional trend of the Ryoke zone in Kinki and Chugoku Provinces) through whole deforming processes. The deformation style of the rocks during the older Ryoke deformation were changed as follows in the younging order: 1) plastic flow on  $S_{1-2}$  (earlier  $B_3$ -substage), 2) deformation related to the formation of the conjugate transversal surfaces  $S_3$  and  $S_4$  (later  $B_3$ -substage) and 3) plastic flow on  $S_{1-2}$ , in some places accompanied with the transversal surfaces  $S_5$  characterized by the preferred orientation of sillimanite grains (Plate 20-3 and 4) ( $B_5$ -substage). However, this does not mean that all the metamorphic rocks in the district had experienced the deformation of those styles progressively. That the plastic flow on  $S_{1-2}$  became active again in the  $B_5$ -substage instead of the deformation related to the  $S_3$ - and  $S_4$ -surfaces seems to reflect the increase of plasticity of the rocks concerned, that is due to the increase of temperature in the metamorphic field depending upon the approach and intrusion of the Sakawa granodioritic rocks in the  $B_5$ -substage. It was concluded that the metamorphic condition, which covered the older Ryoke metamorphic terrain, changed between the  $B_3$ -substage and the  $B_5$ -substage, and that in the  $B_5$ -substage the temperature in the metamorphic terrain was probably higher than that in the  $B_3$ -substage.

The symmetry of movement in each substage of the older Ryoke deformation was roughly monoclinic, and the deformation plane must have had a NNE-SSW strike and approximately vertical dip. The direction of movement seems to have been NNE as a whole.

As read from the geological map of Fig. 3, the geologic structure of the metamorphics and the Sakawa granodioritic rocks is characterized by a large-scale cross-fold. The large-scale cross-fold was produced by the displacement superposed on the structure having an east-west regional trend which had been produced by the older Ryoke deformation. The displacement represents the younger Ryoke deformation. The displacement seems to have taken place in the manner of refolding with vertically plunging axis of external rotation as a whole, accompanied with the formation of the  $B_6$ -folds and  $L_6$ -lineations in each of small fields of the district. The younger Ryoke deformation can be correlated with the approach and forcible intrusion of the batholithic Yagyu granite (the younger granite in the sense of KOIDE).

From the geological outline map of Fig. 2 after NAKAZIMA, in the central part of the Ryoke zone in the Yamato Plateau, principal schistosity and gneissosity surfaces of the Ryoke metamorphic rocks and the older Ryoke granitic rocks and flow layers of the younger Ryoke granitic rocks appear to form dome- and basin-like structures. The large-scale cross-fold in the Kasagi district corresponds to a part of those structures. The older Ryoke granitic rocks in the Yamato Plateau develop as large folded sheet-like masses, as read from the map of Fig. 2. While, the younger Ryoke granitic rocks develop as stock-like or batholithic masses.

On the basis of the conclusions about the genetic history of geologic structure of the Kasagi district, following inferences about geologic structure of the Ryoke zone in the Yamato Plateau can be drawn. The geosynclinal Palaeozoic deposits had suffered the Tamba deformation and had been folded with the *b*-kinematic axis having east-west regional trend, accompanied with the formation of slaty cleavage, (the formation of the Tamba folded mountain), before the Ryoke metamorphism and plutonism took place. The later events were superposed on the rock- and geologic structures formed by Tamba deformation. Judging from the deformation style of the rocks during the Tamba deformation, it can be pointed out that the Ryoke metamorphism began in the field corresponding to the upper horizon of the orogenic mountain. The older Ryoke metamorphism took place in close connection with the older Ryoke deformation with the *b*-kinematic axis having east-west regional trend. Although the older Ryoke deformation (related deformative stress) was superposed upon the Tamba folded mountain, the presence of the boundary line between the Tamba zone and the Ryoke zone drawn at present on the basis of evidences mentioned in preceding pages represents that the older Ryoke deformation was not uniformly superposed all over the zone within which the Tamba deformation took place, but that it was concentrated in the zone within which the regional uprising of isothermal surface related to the older Ryoke metamorphism had taken place. In the later stage of the older Ryoke deformation, the older Ryoke granitic rocks were intruded forcibly as large sheet-like masses. In the next stage, the forcible intrusions of the younger Ryoke granitic rocks as batholithic masses took place and gave rise to the dome- and basin-like structures. This is the younger Ryoke deformation.

Summaries of the results of detailed examinations of the mica and quartz fabrics and petrofabric meanings deducible from them are referred to the Chapter V.

#### REFERENCES

- ARITA, T., (1949): On the Kasagi granitic intrusives and the related metamorphic complex, Yamato district, Japan. *Jour. Geol. Soc. Japan*, 55, (647), 99-104.
- BANNO, S. and MILLER, J., (1961): New data on the dating of the Ryoke and Sambagawa rocks (in Japanese). *Kagaku*, 31, (144).
- BILLINGS, M. P., (1942): *Structural Geology*. New York Prentice-Hall, Inc.
- FAIRBAIN, H. W., (1949): *Structural Petrology of Deformed Rocks*. Cambridge.
- GAULT, H. R., (1945): Petrography, structures, and petrofabrics of the Pinckneyvill quartz-diorite, Alabama. *Geol. Soc. America Bull.*, 56, 181-246.
- GRIGGS, D. T., TURNER, F. J. and HEARD, H. C., (1960): Deformation of the rocks at 500° to 800°C. *Geol. Soc. America Mem.*, 79, 39-104.
- GORAI, M., (1952): The formation of the Japanese Islands (in Japanese). *Shizen*, 7.
- HARA, I., (1959): Relation between folding and plutonism in the Ryoke metamorphic zone of the Kasagi district, Southwest Japan (abstract in Japanese). *Jour. Geol. Soc. Japan*, 65, (766).
- , (1960): Study on the metamorphic conditions of the Ryoke metamorphic rocks (on the viewpoint of petrotectonics) of the Kasagi district, Southwest Japan (abstract in Japanese). *Jour. Geol. Soc. Japan*, 66, 449.
- , (1961): Dynamic interpretation of the simple type of calcite and quartz fabrics in the naturally deformed calcite-quartz vein. *Jour. Sci. Hiroshima Univ., Series C*, 4, (1), 35-53.

- HARKER, A., (1932): *Metamorphism*. London.
- HAYAMA, Y., (1960): Geology of the Ryoke metamorphic belt in the Komagane district, Nagano Prefecture, Japan. *Jour. Geol. Soc. Japan*, 66, (773), 81-101.
- ICHIKAWA, K., (1958): Bemerkung zum tektonischen Werdegang Sudwestjapans während des Paläozoikums. *Jour. Inst. Polytechnics, Osaka, Series G*, 3, 1-13.
- INGERSON, E., (1936): Fabric analysis of a coarsely crystalline polymetamorphic tectonite. *Amer. Jour. Sci. Vth Ser.*, 31, 161-187.
- JONES, K. A., (1959): A petrofabric method of fold analysis. *Amer. Jour. Sci.*, 257, (2), 138-143.
- KARAKIDA, Y. and GOTTFRIED, D., (1961): Lead-alpha dating of some granitic rocks in Kita-Kyushu and some Ryoke granitic rocks (abstract in Japanese). *Jour. Geol. Soc. Japan*, 67, (790), 420.
- KOBAYASHI, T., (1941): The Sakawa orogenic cycle and its bearing on the origin of the Japanese Islands. *Jour. Fac. Sci. Univ. Tokyo, Sect 11*, 5.
- KOIDE, H., (1949): Dando grandioritic intrusives and their associated metamorphic complex (abstract in Japanese). *Monograph Assoc. Geol. Collab.*, 1.
- , (1958): Dando granodioritic intrusives and their associated metamorphic complex. *Japan, Soc. Pro. Sci.*
- KOJIMA, G. and OKAMURA, Y., (1951): Yanai district (in Japanese). *Guide-book of the excursion at the 59th Ann. Meet. of Geol. Soc. Japan*.
- , (1953): Contributions of the knowledge of mutual relations between three metamorphic zones of Chugoku and Shikoku, Southwestern Japan, with special reference to the metamorphic and structural features of each metamorphic zone. *Jour. Sci. Hiroshima Univ., Series C*, 1, (3), 17-44.
- KUNO, H., (1960): Potassium-argon dating of some Japanese rocks. *Kagaku*, 31, (1), 13-17.
- KVALE, A., (1953): Linear structures and their relation to movement in the Caledonides of Scandinavia and Scotland. *Geol. Soc. London Quart. Jour.*, 109, 51-73.
- LÄBURNER, J., (1954): Beiträge zur Typisierung von Quarzfalten. *Tschermaks Miner. u. Petrog. Mitt. Bd. II*, (3), 47-66.
- MATSUSHITA, S., (1950): Geology of Kyoto Prefecture (in Japanese). *Science of the Earth*. 2.
- MCINTYRE, D. B., (1951): Note on the tectonic style of the Ord Ban Quartzites Mid-Strathpey. *Geol. Mag.* 88, (1), 50-54.
- NAKAZIMA, W., (1960): Geology of the northern margin of the Ryoke zone in the Yamato Plateau (in Japanese). *Earth Science*, (49), 1-14.
- OKAMURA, Y., (1957): Structure of the Ryoke metamorphic and granodioritic rocks of the Yanai district, Yamaguchi Prefecture (in Japanese). *Jour. Geol. Soc. Japan*, 63, (747), 684-697.
- , (1960): Structural and petrological studies on the Ryoke gneiss and granodioritic complex of the Yanai district, Southwest Japan. *Jour. Sci. Hiroshima Univ., Series C*, 3, (2), 143-213.
- OKI, Y., (1958): Thermally metamorphosed rocks in the northern Kiso Mountain-Range, Central Japan. (in Japanese). *Jour. Geol. Soc. Japan*, 64, (748), 1-12.
- RAST, N. and PLATT, J. I., (1957): Cross-folds. *Geol. Mag.*, 82, (2), 159-167.
- SANDER, B., (1930): *Gefügekunde der Gesteine*. Wien, Springer.
- , (1948): *Einführung in die Gefügekunde der geologischen Körper*. Ier Teil, Allgemeine Gefügekunde und Arbeiten im Bereich Handstück bis Profil. Wien und Innsbruck.
- , (1950): *Einführung in die Gefügekunde der geologischen Körper*. Iier Teil, Die Korngefüge. Wien und Innsbruck.
- SITTER, L. U. De, (1956): *Structural Geology*. New York.
- WUNDERLICH, H. G., (1959): Erzeugung engständiger Scherflächen in plastischen Material. *Neues Jahrb. Geol. Paläontol. Mh.*, 34-44.
- YAMASHITA, N., (1957): *The Mesozoic System in Japan* (in Japanese). Assoc. Geol. Collab.
- ZOZMANN, I. S., (1955): Gefügeanalysen an Quarzfalten. *Neues Jahrb. Miner.* 87, (3), 321-350.

#### EXPLANATION OF PLATE

- FIG. 1 Profile of the  $B_1$ -folds in metamorphic derivatives from banded chert (from Subarea A).
- FIG. 2 Relation between the  $B_1$ -folds and the principal schistosity surface  $S_{1-2}$  in metamorphic derivatives from banded chert (from Subarea A).
- FIG. 3 The  $S_{1-2}$ -surfaces cutting across the bedding surfaces  $S_1$  in sample of Fig. 2.



FIG. 1



FIG. 2

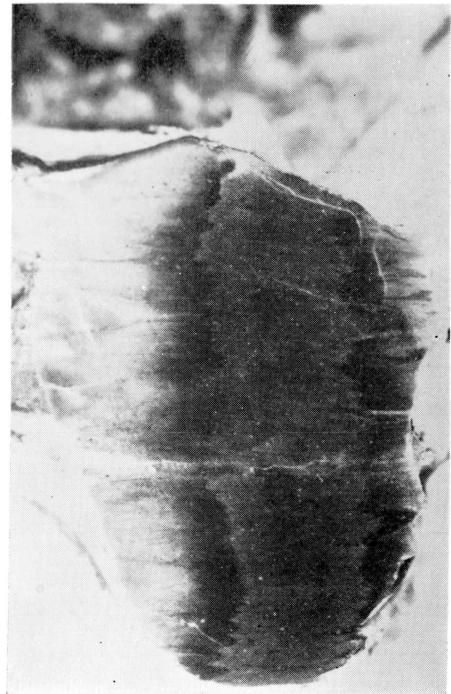


FIG. 3

### EXPLANATION OF PLATE

- FIG. 1 The transversal surface  $S_3$  in pelitic schistose hornfels (from Subarea C). Lower nicol only.  $\times 20$   
FIG. 2 The transversal surface  $S_3$  in pelitic schistose hornfels (from Subarea C). Lower nicol only.  $\times 20$   
FIG. 3 The transversal surface  $S_3$  in pelitic gneiss (from Subarea K).  $\times 2$   
FIG. 4 Disharmonic fold of pelitic gneiss (subarea K).  $\times 1$

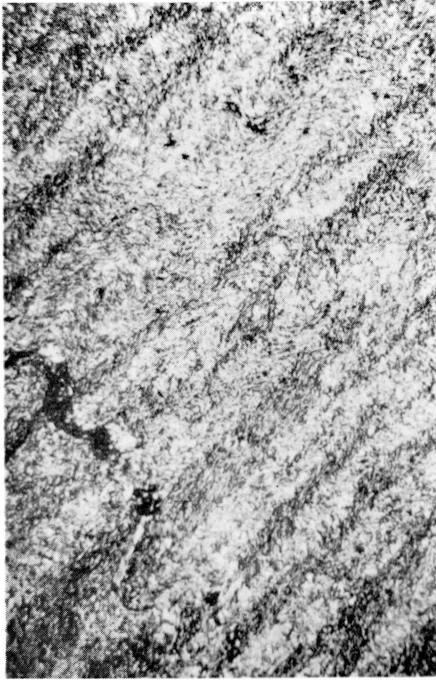


FIG. 1



FIG. 2



FIG. 3

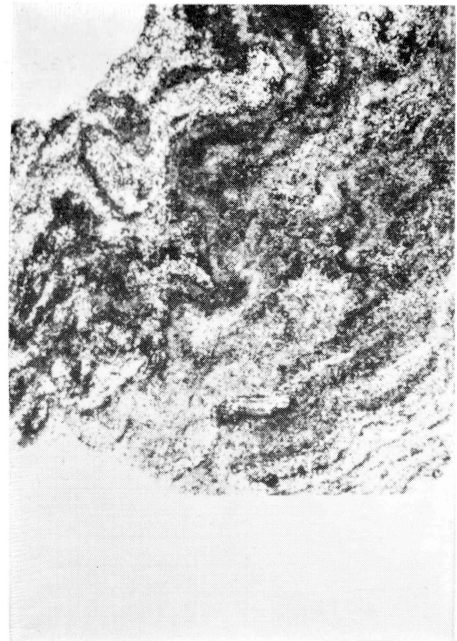


FIG. 4

### EXPLANATION OF PLATE

- FIG. 1 Transversal surface  $S_5$  in pelitic gneiss (from Subarea K).  $\times 1.2$
- FIG. 2 Zone of the  $S_5$ -surfaces partially granitized (in pelitic gneiss from Subarea K).  $\times 1$
- FIG. 3 Sillimanite grains preferably orienting on the  $S_5$ -surfaces in the thin section parallel to  $L_5'$ . Lower nicol only.  $\times 35$
- Fig. 4 Sample of Fig. 3 photed in the thin section perpendicular to  $L_5'$ . Lower nicol only.  $\times 35$



FIG. 1

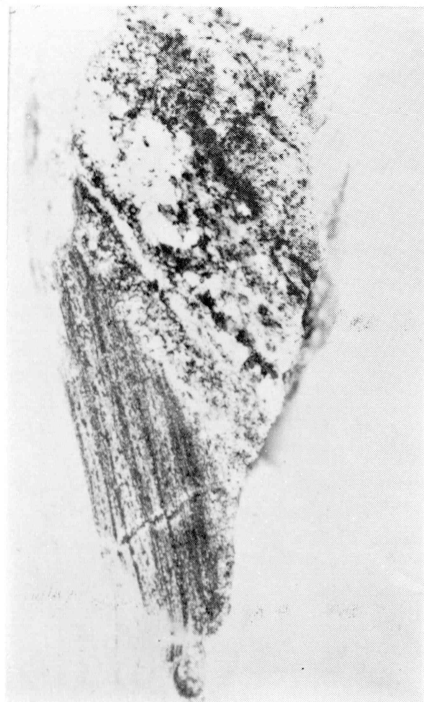


FIG. 2

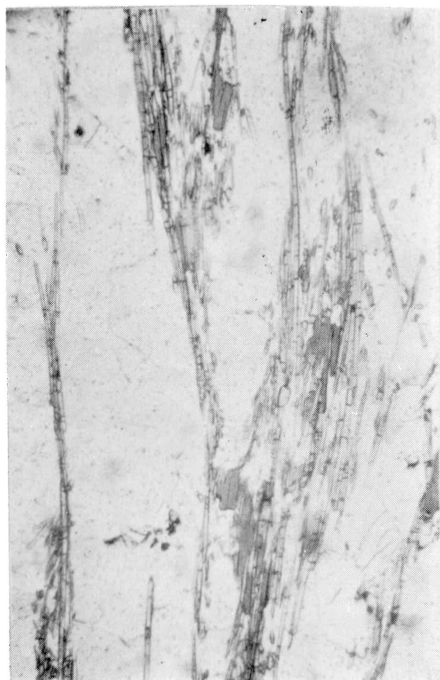


FIG. 3



FIG. 4